This is to certify that the

thesis entitled

PYROLYSIS AND CATALYTIC GASIFICATION
OF POPLAR SPP

presented by

Mark Roger Boyd

has been accepted towards fulfillment
of the requirements for

Master's degree in Chemical Engineering

Major professor

Date October 4, 1979

OVERDUE FINES ARE 25¢ PER DAY
PER ITEM

Return to book drop to remove
this checkout from your record.

PYROLYSIS AND CATALYTIC GASIFICATION OF POPLAR SPP

By

Mark Roger Boyd

A THESIS

Submitted to
Michigan State University
in partial fulfillment of the requirements
for the degree of

MASTER OF SCIENCE

Department of Chemical Engineering

1979

ABSTRACT

PYROLYSIS AND CATALYTIC GASIFICATION
OF POPLAR SPP

By

Mark Roger Boyd

Two salts, Na_2CO_3 and K_2CO_3, have been investigated to determine their catalytic effects on pyrolysis and gasification of Poplar SPP and char derived from Poplar SPP. A differential reactor was used with temperatures ranging from 550° to 700°C, space velocities of 2 to 7.25 s^{-1}, and steam partial pressures of 45 to 100 kPa.

Pyrolysis has been found to be nondestructive to the basic cell structure of wood, except when impregnated with an alkali salt. Pyrolysis products are CO, CO_2, and CH_4.

The char gasification rate law observed from steam partial pressure data is

$$\text{Gasification rate} = k \exp(-E_a/RT)\, p_{H_2O} \frac{\text{g - moles}}{\text{g C} \cdot \text{min}}$$

Preexponential factors of 10.7 and 16.4 g - moles/g C min kPa and activation energies of 89.2 and 94.2 kJ/mole were observed for the catalytic gasification of char using Na_2CO_3 and K_2CO_3, respectively. Char gasification products were H_2, CO, CO_2, and CH_4. Rates were compared considering methane as derived from carbon monoxide as opposed to the product of direct hydrogenation of carbon.

Intraparticle diffusion becomes substantial for particles over 1.0 cm. Conversion of steam is not sensitive to mixing conditions within a tubular flow reactor.

To my parents

ACKNOWLEDGEMENTS

The author would like to express his appreciation to his academic advisor, Dr. Martin C. Hawley, for his encouragement and assistance. Also to Dr. Antonio Devera for his advice and guidance during the study. The author also wishes to thank Mr. Don Childs for his invaluable assistance in constructing and assembling the experimental apparatus, and Dr. John Young of Argonne National Laboratory for timely advice on engineering the experimentation. Appreciation is also extended to Dr. James Hanover for his valuable expertise, and Robert Konopacz for obtaining the electromicrophotographs.

The encouragement and support of the author's wife, Anita, is also sincerely appreciated.

TABLE OF CONTENTS

	Page
LIST OF TABLES	vi
LIST OF FIGURES	vii
NOMENCLATURE	ix
INTRODUCTION	1
PHYSICAL AND CHEMICAL PROPERTIES OF POPLAR SPP	6
PYROLYSIS AND GASIFICATION BACKGROUND	14
Pyrolysis	14
Gasification of Carbon and Char	24
Early Pyrolysis and Gasification Experiments	32
EXPERIMENTAL CONDITIONS	39
Introduction	39
Reactant Gas Production	40
Reactor Assembly	42
Product Gas Processing	44
Gas Analysis	45
Sample Preparation	46
Operating Procedure	47
EXPERIMENTAL RESULTS	49
Effects of Pyrolysis	49
Salt Catalyzed Wood Char Gasification	53
MODELING	64
Single Particle Effectiveness Factor	64
Tubular Reactor Axial Dispersion Model	71

Page

SUMMARY AND CONCLUSIONS 81

Conjectures on Catalytic Activity 81
Observations and Comments 82

APPENDICES 86

APPENDIX A: Future Work 87

APPENDIX B: Sample Rate Calculation 90

APPENDIX C: Effectiveness Factor Calculation . . 94

APPENDIX D: Summary of Rate Data 97

BIBLIOGRAPHY 101

LIST OF TABLES

Table		Page
1.	Summary of pyrolysis investigation	15
2.	Summary of carbon gasification investigation .	25
3.	Summary of rate data	98

LIST OF FIGURES

Figures		Page
1.	Microphotograph of Poplar at 200 magnification	7
2.	Schematic of section A in Figure 1 showing components of cell wall structure	8
3.	Chemical structure of (a) cellulose and (b) hemicellulose	11
4.	Chemical structure of lignin	13
5.	Reaction mechanism of char gasification	28
6.	Observed gas flow from pyrolysis of K_2CO_3 impregnated wood	36
7.	Schematic of experimental apparatus	41
8.	Picture of reactor assembly showing main reactor tube and steam preheater	43
9.	Picture of reactor assembly	43
10.	Electromicrophotograph of Poplar SPP	50
11.	Electromicrophotograph of Poplar SPP after 1 minute of pyrolysis	50
12.	Electromicrophotograph of Poplar SPP after 4 minutes of pyrolysis	51
13.	Electromicrophotograph of Poplar SPP after 8 minutes of pyrolysis	51
14.	Effect of steam partial pressure on reaction rate calculated from CO and CO_2, case A	57
15.	Effect of steam partial pressure on reaction rate calculated from CO, CO_2 and CH_4, case B	58
16.	Activation energy plot, ℓn rate versus 1/T	60

Figures Page

17. Effect of space velocity on reaction rate at 625°C for uncatalyzed material only 62

18. Drawing of flat slab geometry for a particle with external bulk film resistance 65

19. Plot of effectiveness factor versus particle size, k = 1.519 s^{-1}, $\mathcal{D}_e$ = 3.19 cm^2/s . . . 68

20. Comparison of effectiveness factor for catalyzed (k = 1.519 s^{-1}) and uncatalyzed (k = 1.14 s^{-1}) char, $\mathcal{D}_e$ = 3.19 cm^2/s 70

21. Drawing of a plug flow reactor showing a differential element 72

22. Plot of 1 - X versus Peclet number. $\mathcal{D}_e$ = 3.19 cm^2/sec, k = 1.519 sec^{-1}, L = 40 cm, v = 40 cm/s, D_p = 0.5 cm 74

23. Plot of 1 - X versus Peclet number. $\mathcal{D}_e$ = 3.19 cm^2/sec, k = 1.519 sec^{-1}, L = 40 cm, v = 40 cm/sec, D_p = 1.0 cm 75

24. Plot of 1 - X versus Peclet number. $\mathcal{D}_e$ = 3.19 cm^2/sec, k = 1.519 s^{-1}, L = 40 cm/sec, D_p = 2.0 cm 76

25. Plot of 1 - X versus Peclet number, $\mathcal{D}_e$ = 3.19 cm^2/sec, k = 4.464 s^{-1}, L = 40 cm, v = 40 cm/sec, D_p = 1.0 cm 77

26. Effect of residence time of steam on conversion, $\mathcal{D}_e$ = 3.19 cm^2/sec, k = 1.519 s^{-1}, L = 40 cm, D_p = 1.0 cm 79

27. Effect of effective diffusivity on conversion. k = 1.519 s^{-1}, L = 40 cm, v = 40 cm/sec, D_p = 1.0 cm 80

NOMENCLATURE

Bi_m = Biot mass number, dimensionless, $\frac{k_g L}{\mathcal{D}_e}$

C_i = Concentration of species i, gr - mole/cm^3

$D_{i,j}$ = Bulk diffusion coefficient of component i in j, cm^2/sec

$\mathcal{D}_{e_i}$ = Effective diffusivity coefficient of component i, cm^2/sec

D_a = Damkohler number, dimensionless, $\eta k \frac{L}{v}$

f = Dimensionless concentration

k = reaction rate constant, s^{-1}

L = Length, cm

Pe = Peclet number, dimensionless = $\frac{vL}{D_z}$

s = Dimensionless distance within the reactor

X = conversion of steam

Y_i = Mole fraction of component i

z = distance, cm

ψ = Dimensionless concentration

ξ = Dimensionless distance

ϕ = Thiele modulus, dimensionless

η = Effectiveness factor

ε = Void fraction

INTRODUCTION

Gasification technology can be applied to biomass to produce synthesis gas, a mixture of CO and H_2, which can be converted to a variety of fuels and chemicals. The objectives of this research are to determine and model physical and chemical changes which occur during high temperature pyrolysis and gasification of biomass. The kinetic parameters determined by the study can be coupled with mass transfer knowledge to describe and design the characteristics of a biomass gasifier. The size, pore structure, and composition of the biomass feedstock will all have significant effects on the rate of gasification and thus, design of commercial gasification units. Biomass gasification may become an important alternative for utilizing solar radiation for production of gaseous and liquid hydrocarbons for fuels and chemicals.

"Biomass potential in 2000 put at 7 quads," is a current concensus among recent estimates (1). This amounts to 10 percent of the current energy consumption rate. Current DOE funding was noted to amount to $26.9 million in 1979 for biomass conversion, which is projected to grow to $118.9 million by 1981. Most economically feasible

projects at this time are processes which produce expensive chemicals. Thermochemical gasification and liquefaction are currently important areas for study. This study is aimed toward defining unknowns related to application of gasification technology to biomass.

Specifically this study is concerned with monitoring physical and chemical changes of Poplar SPP under a variety of gasification conditions. Poplar SPP is a hybrid tree which has, due to its very rapid growth, been singled out as a likely candidate for cultivated biomass plantations. From a few preliminary experiments it was observed that two important processes occur in the gasification of raw biomass, pyrolysis and gasification.

From a process standpoint, gasification of raw biomass into synthesis gas will involve several steps (15): initial devolatilization, pyrolysis, and gasification. Upon being subjected to a high temperature environment (600° to 800°C) a temperature gradient begins to form, up to 100°C, within the particle which quickly devolatilizes any adsorbed water and gases. As the intrapellet temperature gradient continues to increase (100° to 500°C) chemical degradation begins. This process of pyrolysis is the thermal degradation of the wood components into simpler molecules. Wood is composed predominately of hemicellulose, cellulose, lignin, and water. Typically

the water content of green wood is 50 percent by weight. Cellulose, hemicellulose, and lignin are polymeric in nature. Poplar SPP is a typical hardwood which is chemically composed of 48.8 percent cellulose, 19.3 percent lignin, and 29.7 percent hemicellulose, and 1 percent ash. The remaining 1.2 percent is composed of extractives. Decomposition involves first the breakdown of the polymers into monomer units, then the further degradation of the monomer units into an array of decomposition products. The degree of complexity of the final products is a function of the heating conditions, the initial sample size, porosity, and the ash content. The pyrolysis products may also interact during the decomposition to form an even greater variety of products. Termination of this stage of the reaction sequence leaves a residual char composed mainly of carbon. Further heating of char will not produce any more gaseous or liquid components. The residual char can be gasified or reacted with steam at 500°C and higher to produce synthesis gas. This process for wood char gasification is similar to coal gasification, but is somewhat different due to pore structure and ash content. Important parameters for the steam carbon reaction are steam partial pressure, temperature, and catalyst impregnation.

Previous workers (17, 21, 22) have observed that impregnation of the biomass with potassium and sodium salts catalyzes the pyrolysis and gasification reactions. The experimental work of this study includes pyrolysis and gasification of nonimpregnated and salt impregnated biomass samples. Catalyst activity was investigated to determine effects on morphological structure during pyrolysis, pyrolysis rate, and gasification rate.

Pyrolysis experiments were performed at temperatures ranging from 400° to 700°C. Space velocity of the pyrolysis gas was 4 sec^{-1} based on a sample volume of approximately 60 cm^3 (five to seven grams of finely ground particles) and a volumetric reactant gas flow of 240 cm^3/sec.

The final set of experiments performed were the measurements of reaction rates of catalyzed pyrolysis char. For these experiments, finely divided one to two mm particles of Poplar SPP were subjected to pyrolysis for 10 minutes to produce char for the gasification experiments. The resultant char was then impregnated with a catalyst, and gasification reaction rates of the resultant material determined for values of steam partial pressure between 45 and 100 kPa, and steam temperatures between 550°C and 700°C. These experiments were modeled and the kinetic constants were determined. The kinetic constants along

with estimates of mass transfer parameters were used to model more complex reactor systems.

The original objective of this study was to gasify raw wood and model the process. However, after a series of preliminary experiments it was found that the liquid products of the pyrolysis process were too difficult to handle in a quantitative manner with our experimental apparatus. Therefore it was decided to examine the gasification of the residual char, which is a much cleaner process. The experimental work was done jointly with Mr. Craig Anderson. Experiments were done on both salt impregnated and nonimpregnated wood char samples. Results of the nonimpregnated experiments are reported in Mr. Anderson's thesis. This thesis reports details of gasification experiments for salt impregnated wood char and comparisons are made with the nonimpregnated results. This report also deals with some qualitative results of the preliminary pyrolysis experiments.

PHYSICAL AND CHEMICAL PROPERTIES OF POPLAR SPP

The cellular structure of poplar wood is shown in Figure 1. The major distinquishable features are the parallel, closely packed cells. The intracellular substance is composed predominately of amorphous lignin. The cell walls are divided into two main parts as can be seen in Figure 2. The primary wall (P) is an amorphous collection of microfibrils which are essentially noncrystalline. The secondary wall is subdivided into the following three parts: (a) the outer layer (S1) which contains a large number of cross hatched fibrils, (b) the middle layer (S2) of the inner wall which constitutes the largest percentage of the cell wall volume, and (c) the inner layer of the secondary wall (S3). The S2 layer is composed of a large number of parallel fibrillar units oriented at a slight angle to the cell axis. The S3 layer is composed of parallel fibrils formed in a flat helix, nearly perpendicular to the fibrils of the S2 layer.

The microfibrils are the basic physical entity in the cell wall construction. They are thin rods

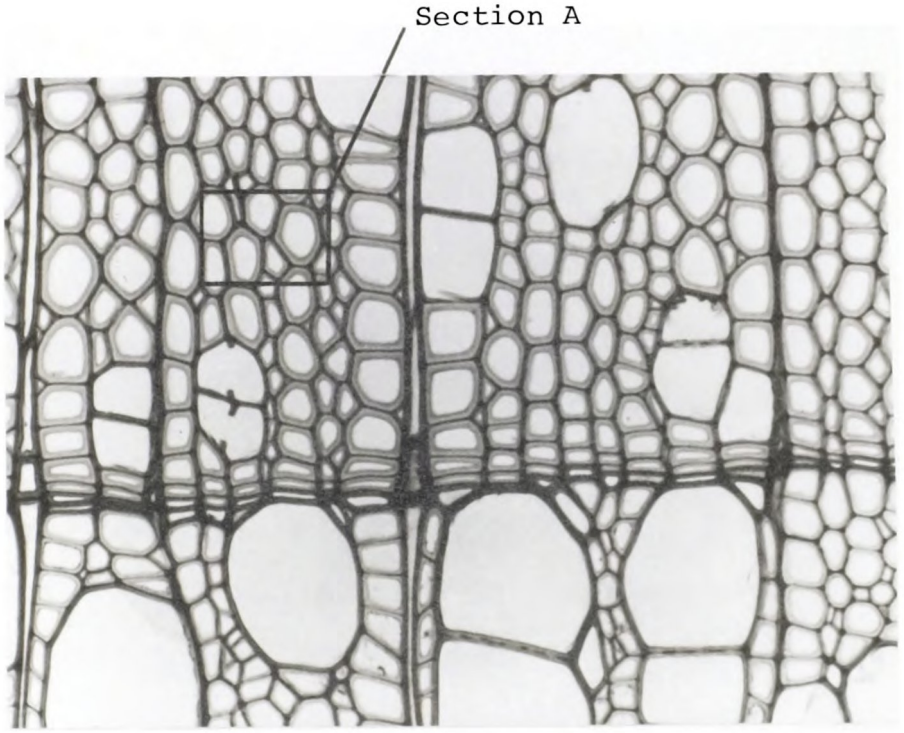

Figure 1.--Microphotograph of Poplar at 200 magnification.

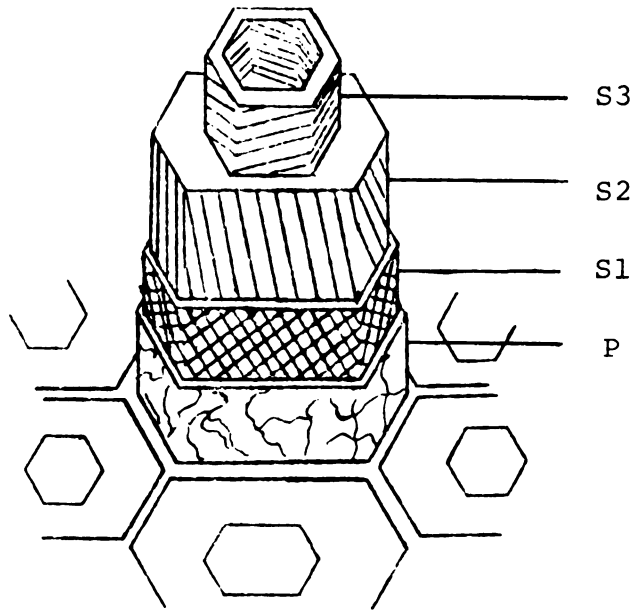

Figure 2.--Schematic of section A in Figure 1 showing components of cell wall structure.

approximately 5 to 10 ηm in diameter. Theories from as recently as 1970 have postulated the physical structure of the fibrils as alternating crystalline and amorphous regions. The highly crystalline regions are believed to be more pure in D-glucose than the amorphous regions which may contain high percentages of other sugar molecules. The actual polymeric compositions of the three different walls do not vary substantially. The primary distinguishing feature of the walls is the contrasting orientation of the microfibrils. X-ray data have shown (21) that there must be some type of crystalline imperfections in the fibrils, but whether or not they are in discrete locations or homogeneous throughout the structure is not yet known.

The cellulosic fibrils imbedded in a matrix of lignin and hemicellulose should provide a relatively high permeability barrier against radial diffusion. The ratio of axial to radial permeability of raw wood is over 100 (23). This property is important during pyrolysis and gasification of wood in a reactor, especially during the stages of decomposition in which the original physical structure remains primarily intact.

As was stated previously, the polymeric compositions of the three different cell walls do not vary substantially. This leads to the fact that the chemical

nature of wood is quite uniform throughout the cellular parts. Although uniform in distribution, the chemical makeup of the individual polymers are quite complex.

On a dry basis, Poplar SPP is composed of 48.8 percent cellulose ($C_6H_{10}O_5$), 19.3 percent lignin ($C_{29}H_{36}O_{11}$), 29.7 percent hemicellulose ($C_5H_{10}O_5$), and 1 percent ash. The remaining 1.2 percent is comprised of extractives such as resins, tannins, and other miscellaneous compounds. Ash content is 70 percent potassium, calcium, and magnesium. Molecular structures of cellulose and hemicellulose are illustrated in Figure 3.

Madorsky (9) has shown that under slow heating conditions of 5° to 25°C per minute, less thermally stable C-O bonds which abound on the monomer, break with the result of a breakdown of the individual monomer units which yields water, carbon monoxide, carbon dioxide, and char from the polymer. Under rapid heating conditions, above 25°C temperature rise per minute, more selective breaking of the glycosidic bonds connecting the monomer units occurs leading to the formation of levoglucosan, the primary component of tar or smoke. Hemicellulose is chemically similar to cellulose. Instead of glucose units, xylans constitute the backbone of the polymer. Some of the xylose units carry a single side chain of a glucuronic acid residue. This is illustrated in Figure 3b.

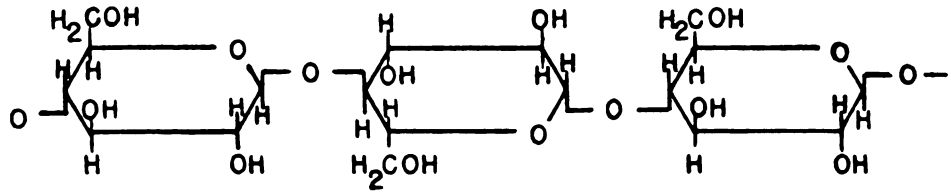

(a) Cellulose

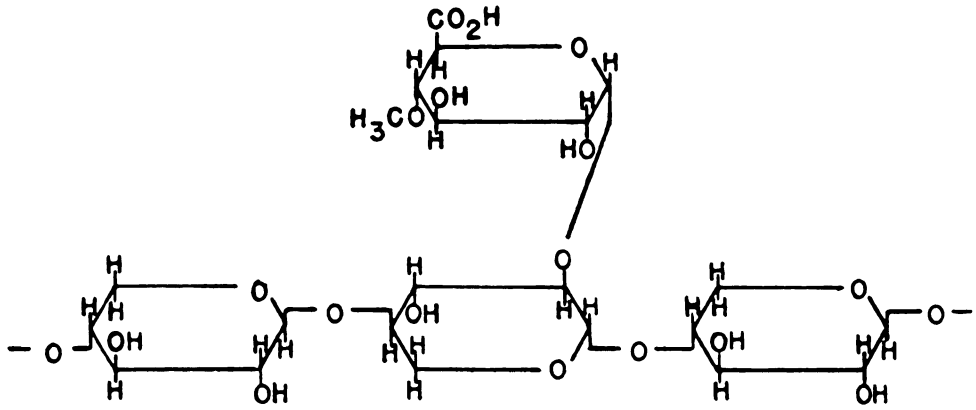

(b) Hemicellulose

Figure 3.--Chemical structure of (a) cellulose and (b) hemicellulose.

Pyrolysis products are similar to those of cellulose except that no levoglucosan formation is possible due to the more compact chemical structure of the monomer units. Therefore hemicellulose does not contribute to production of volatile products significantly. Instead, less gas evolution occurs with a large portion of the material being converted to char.

Lignin (Figure 4) is a polymer composed of highly substituted propylbenzene monomer units. This is the most stable polymer in wood, and is postulated to be the substance which bonds the other polymers together to give wood its strength. Upon decomposition, a wide variety of substituted phenolics are produced. Much of this material volatilizes to tar, but a greater portion contributes to the formation of char.

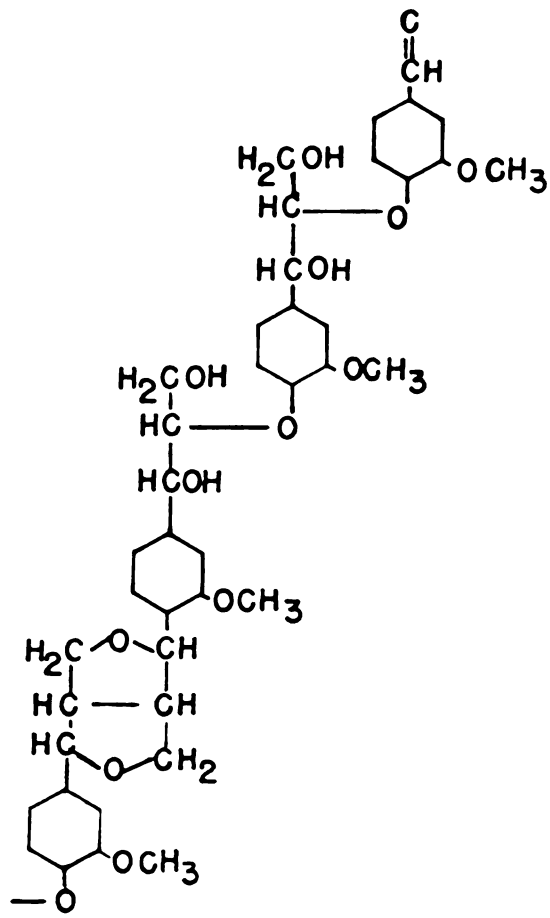

Figure 4.--Chemical Structure of Lignin

PYROLYSIS AND GASIFICATION BACKGROUND

Pyrolysis

Several workers (2-8, 10, 12, 13) have studied pyrolysis of wood and and wood components. Highlights of this work are summarized in Table 1. Brenden (2) discusses briefly the effects of rapid heating (0.5 gram samples of wood subjected to 400° to 800°C) on wood decomposition and found (a) weight loss can be as great as 80 percent, and (b) achieving such weight loss provides gaseous pyrolysis products of high heat content (2312 to 4025 cal/gram). Although no details of the heating periods or rate of temperature increase were presented concisely, this communication supports the fact that high temperature isothermal conditions produce high weight loss and yields products of complicated chemical makeup. Much work has been done on low temperature pyrolysis in the range of 275° to 500°C (3, 4, and 5). Roberts and Glough (3) try to predict the behavior of wood pyrolysis (activation energies and rate constants) over the range 275° to 435°C. Specimens in the study were 2 cm in diameter and 15 cm in length. Experimental procedure involved thermocouple readings at various radii, and

TABLE 1.—Summary of Pyrolysis Investigations.

Reference	Sample Type and Size	Experimentation	Comments/Observations
Brenden (1967)	Ponderosa Pine, 1/4 in diameter, 1 in long, 1/2 gram	Thermogravimetric pyrolysis in Nitrogen, 240°-822°C	Heat of combustion of pyrolysis products is function of volatile fraction
Roberts and Glough (1963)	Beech, 1 cm diameter, 15 cm long	Thermogravimetric pyrolysis in Nitrogen, 275°-435°C	First order kinetics, secondary reactions are important
Kanury (1972)	Woodlike pressed cellulose cylinders, 1.75 cm diameter	Nitrogen flushed pyrolysis cond. X-ray densitometer and internal temp. measurements	First order kinetics E_a = 19 kcal/mole, pyrolysis is function of internal temp. profile
Blackshear and Murty (1965)	Pressed cellulose cylinder, 1 in dia. cylinders	Differential thermogravimetric anal, 100°-800°C burning cond. in air	Internal temperature gradients function of internal mass transfer
Beall (1971)	Cellulose, hemicellulose, lignin prep. and variety of wood, 125-250 μm groundwood	Differential calorimetric analysis, 25°-800°C	Major endothermic peaks at 375°-400°C, exothermic peaks 400°-800°C
Arseneau (1961)	Balsam fir and its components, powdered 70-200 mesh	Differential thermal analysis	Differential thermogram of wood is a composite of the thermogram of its components
Lipska and Parker (1966)	α-cellulose, 2 cm diameter disks	Weight loss measurements, pyrolysis conditions	Rate dependence varies from zero to first order with time
Chatterjee and Conrad (1966)	Cellulose, finely ground and ball milled	Thermogravimetric analysis, 270°-310°C, Helium atmos.	Crystallinity affects kinetics, first order kinetics after 40% conversion
Beall (1969)	Three extracted lignins, 50 mg samples	Dynamic thermogravimetric analysis, 25°-1000°C	Lignin stability related to prep. and molecular wt. Hemicellulose degrades before cellulose
Stamm (1956)	Douglas Fir, sawdust and extracted samples	Air and Nitrogen streams 93.5°-300°C gravimetric analysis	Rate of degradation of wood comp. Hemicellulose > cellulose > lignin

continuous weight loss measurements. No specific conclusions were reached on the physical or chemical nature of pyrolysis. They treated their data according to first order kinetics with respect to weight loss.

$$\ell n \frac{w - w'}{w_o - w'} = -k \int_o^t \exp(-E/RT)\, dt \qquad (1)$$

w' = final weight of specimen
w_o = initial weight of specimen
k = rate constant

Using such sample sizes the author showed that simple pyrolysis kinetics as shown in Equation 1 are too simple a treatment, "since values obtained for the activation energy and heat of reaction vary with experimental conditions." For the early stages of pyrolysis the activation energy was found to be 25 kcal/mole and the rate constant equal to 9.1×10^4 minutes^{-1}. Kanury (4) also examined the limitations of studying pyrolysis of large scale specimens. In-situ measurements and X-ray density measurements were adequate for determining pyrolysis kinetics and a consistent activation energy along the radius of the specimen. Significant observations based on this data are (a) layers of solid lying deeper from the exposed surface exhibit a progressively lower maximum pyrolysis rate and a progressively wider range of temperatures in which pyrolysis occurs, (b) the ratio of the

maximum pyrolysis rate to the temperature at which it occurs is roughly constant, (c) the rate curves near the surface and those near the axis are smooth and regular; those at intermediate locations however, exhibit a constant rate for a certain duration, the length of which increases with depth beneath the exposed surface and then decreases, and (d) the rate curves fall nearly exponentially with time at some radial locations close to the axis.

Blackshear and Murty (5) performed weight loss, and surface and internal temperature measurements on 2.54 cm diameter pressed cellulose cylinders. Accordingly, mass and heat transfer for burning and pyrolyzing solids are coupled with a driving force originating from the decomposition of the cellulose within the sample. The driving force is a function of heating history and sample size. They state that a more elaborate treatment of the transient pyrolysis of cellulose material would result in some sort of size dependency. Experiments were conducted on internal time-temperature histories. The process their data suggests is one in which gas is evolved below the surface first endothermically (500°C). The same process occurs near the surface as well, but is augmented by further heat release when vapors from lower regions undergo a secondary pyrolysis, this time an exothermic

one, as they pass through the hot outer char layer. Such a picture is in agreement with the results of Roberts and Glough. A significant conclusion in their paper states that internal energy transport (probably in the form of pyrolysis products) will be directly affected by diffusion and convection of mass within the pyrolyzing solids and must be considered when formulating a mathematical description of the process. The chemical interaction of the pyrolysate gases and the char should also be considered. All previous papers (2, 3, 4, 5) point out the significance of heating conditions, and the coupled effects of heat and mass transfer on predicting the nature of wood pyrolysis on a large scale.

Intrinsic phenomenon of thermal degradation of wood and its components has also been the subject of intense interest, especially to those involved in the studies of flame prevention. Beall (6) observed two major features of the aforesaid temperature phenomenon. One endothermic peak was apparent at 375° to 400°C and a larger exothermic peak from DTA was observed from 400° to 800°C. These were accounted for as the thermal breakdown of the primary material, and chemical interaction of the pyrolysis products, respectively. Aside from a few insignificant aspects, the thermogram of wood is largely a product of the individual components (lignin, hemicellulose, and

cellulose). Arseneau (7) examined the thermal breakdown of balsam fir and its components in air from 50° to 420°C. His conclusion states that "the differential thermogram for balsam fir when heated in air is simply a composite of the individual thermograms of the various components of the wood, with little, if any, interaction between the components."

Based on this information, data on the pyrolysis of wood components may shed some information on wood pyrolysis. Lipska and Parker (8) analyzed kinetics of cellulose in the range of 250° to 298°C. Different types of rate dependence were found for different time intervals: (a) an initial period of rapid decomposition and weight loss, (b) a range in which both the volatilization and decomposition are of zero order, and (c) a region in which the volatilization follows a first order rate, leaving a char deposit which does not undergo further pyrolysis. An additional observation states that the degree of decomposition and volatilization occuring during the zero order phase increases with increasing temperature. An activation energy of 175.8 kJ/mole applies to the decomposition rates in the zero order range. Analysis of the remaining glucosan content shows no readily hydrolyzable material remaining after 75 percent weight loss. Weight loss data show a consistent value of 15 percent

residual material remaining. An important point to note is the elemental compositions of the remaining char heated at 500°C, 98 percent carbon and 2 percent hydrogen. Elemental analysis was not done as a function of time, though it might be instructive to determine the rate of oxygen loss as compared to carbon. This information might infer something about the process of molecular breakdown.

A majority of the weight loss observed in cellulose can be explained by an observation made by Madorsky (9) where 37 percent of a cellulose sample was converted to levoglucosan. Madorsky accounted for this by random scission of 1,4 glycosidic linkages to selectively produce levoglucosan.

$$(C_6H_{10}O_5)_n \longrightarrow n\ \underset{\text{levoglucosan}}{C_6H_{10}O_5} \qquad (2)$$

Other workers have also reported high percentages of levoglucosan yields (Conrad and Chatterjee, 10). Weight loss may actually be controlled by larger morphological influences according to ideas postulated by Golova, Krylona, and Daklady (11). They note such influences as degree of crystallinity, length of polymer constituents, and other macroscopic properties in the structure of the cell wall. Chatterjee and Conrad (10) studied the kinetics of cellulose decomposition in the range of 270° to 310°C.

They observed a complex reaction rate behavior up to 60 percent conversion between the temperature range of 270° to 350°C. Beyond this a slow weight loss was observed beginning at 360°C and lasting until 450°C. This latter stage was considered the decomposition of the residual material. Two activation energies were found for the initial degradation (levoglucosan formation) of 138 kJ/mole for adsorbent cotten, and 157 kJ/mole for ball milled cotton. These differences also suggest that morphological structure of the polymeric material may affect the decomposition process. The authors make an important note concerning their investigations as opposed to other studies. In their technique the temperature was gradually raised from ambient to the specified, thereby avoiding the problem of a time lag while a temperature profile forms within the material. The author believes that the thermal lag inherent in isothermal experiments introduces error in the rate data during the initial period of exposure. It is certainly true that divorcing the aspects of kinetics from temperature-time histories will certainly lead to different results, since they are directly related.

As for the other components of wood, Beall (12) observed the maximum temperatures in which lignin is thermally stable is 450°C. Major products formed are largely substituted phenolics from the monomer units

comprising the polymeric lignin. Stamm (13) observed a lower degradation temperature for hemicellulose of 260°C, and an activation energy of 111.7 kJ/mole in a range of 110° to 220°C. He also stated that hemicellulose degrades four times faster than wood, and lignin only one half as fast as wood.

In any case, the decomposition of wood will be somewhat more complex than that of cellulose. Shafizadeh (14) presented a schematic of the general pyrolysis reactions of cellulose.

$$(C_6H_{10}O_5) \longrightarrow \begin{cases} CO,\ CO_2,\ H_2O,\ C \\ \text{levoglucosan} \\ \text{combustible volatiles} \end{cases} \qquad (3)$$

Also, very rapid high temperature heating is responsible for the following variety of products reported by Shafizadeh.

$$\text{hemicellulose} \longrightarrow CO,\ H_2,\ CH_3CO_2H,\ CH_2O \qquad (4)$$

$$\text{lignin} \longrightarrow \text{substituted phenolics},\ CO_2,\ CO,\ CH_4,\ C_2H_4,\ C_2H_6,\ HCHO,\ CH_3CHO \qquad (5)$$

As pointed out by Shafizadeh (14) "the difficult task of extending the data obtained on cellulose to wood and plant materials is further complicated by the paucity

of information on the pyrolytic reactions of hemicellulose and lignin." Beall (12) reported TGA analysis of wood lignin and hemicelluloses over the temperature range of 25° to 1000°C at 6°C/min. This is a very slow heating rate in terms of what might be called rapid pyrolysis (25° to 100°C per minute). All of his curves showed 50 percent pyrolysis between 350° to 450°C and nearly complete pyrolysis by 600°C. Fifty percent pyrolysis of hemicellulose occurs between 250° to 300°C, with nearly complete pyrolysis by 600°C. Also, extracted hemicellulose material showed greater thermal stability. Activation energies of lignins of 46 to 75 kJ/mole were observed to increase with temperature. They reported that hemicelluloses displayed somewhat higher activation energies of 104 to 125 kJ/mole.

Many of the previous researchers have attempted to apply some rate behavior to the pyrolysis process, which is the complex combination of numerous reactions and the subsequent mass transfer of the reaction products from the reacting material. Rate determinations are largely based on thermogravimetric data which inherently lump both reaction and mass transfer steps together. Describing the complex pyrolysis process by the observation of one variable, such as weight loss, certainly masks many less easily observable physical and chemical changes.

A better approach would be to more discretely define possible reaction pathways, perhaps incurred from populations of functional groups and bonds within the reacting material, similar to the interpretation of catalytic cracking reactions of petroleum refining, then couple this reaction approach with plausible mass transfer mechanisms of the pyrolysis products through the surrounding medium. An improved characterization of the overall process by fundamental chemical engineering principles would prove far more valuable to the application and design of biomass gasifiers, and may provide substantial insight into the apparent diversity of information already assembled. This fundamental approach may possibly integrate the effects of catalyst impregnation in a more readily distinguishable manner.

Gasification of Carbon and Char

Several workers (16-20) have studied gasification of carbon and char. Important aspects of their work are summarized in Table 2, and details are presented in the following discussion.

Blackwood and McGrory (16) examined carbon reactions with steam at pressures up to 5 MPa, and in the temperature range of 750° to 830°C. A differential reactor was used. Low ash content carbon was obtained by

TABLE 2.--Summary of Carbon Gasification Investigation

Investigator	Sample Type and Size	Experimentation	Conclusions
Blackwood and McGrory (1958)	-7 +14 B.S. sieve coconut charcoal	Differential packed bed reactor	Number of reactive carbon sites constant with time
Lewis, Gilliland, and Hipkin (1953)	100 gram samples, wood charcoal	Fixed bed reactor, 750 psi, 1200°F	Reaction rate at 600°C, 7 to 40 times higher than expected using K_2CO_3
Stern, Loguidice, and Heinemann (1965)	Sugar and sugar charcoal, softwood sawdust; 1.5 to 2.5 gram samples	Continuous packed bed reactor 1000°C	High temperature catalytic cracking produces 50/50 mole % CO and H_2 mixture
Walkup et al. (1978)	Lodgepole wood, 15 gram samples impregnated with Na_2CO_3	Continuous bench scale reactor, 750°C	Addition of alkali carbonate decreases tar production and enhances rate of gasification. H_2 concentration low in the absence of steam.

pyrolysis of coconut carbon and extraction with hydroflouric and hydrochloric acid. This procedure was necessary to eliminate any ash which might catalyze the water gas shift reaction. Although this precaution was taken, CO_2 still remained in the effluent as a product gas. This necessitated calculating the reaction rate from the total oxides of carbon produced. Only a small amount of methane was formed at atmospheric pressure, and this was thought to be due to a side reaction between carbon and hydrogen. However, as will be seen from our work, results indicate this may not be true. Only uncatalyzed materials were studied. The material had a bulk density of 0.5 g/cm^3, and a size of -7+14 B.S. sieve. Two important effects were observed: (a) varying the space velocity from 2 to 15 sec^{-1} showed no effect of external mass transfer control; a slight increase in observed rate with space velocity was explained by changing temperature conditions in the reactor as the steam flow was increased, and (b) the rate of gasification was found to be a function of conversion, though not appreciably. No significant change of reaction rate with conversion was observed up to 20 percent conversion. Maximum deviation of the rate was 5 percent after 50 percent conversion. Considering the constant reaction rate, the authors presume that the total number of sites in the char remained fairly constant with

time. Carbon atoms on the edge of the cyrstal lattice having one free orbital may combine with the oxygen to form carbon monoxide. Subsequent removal of the carbonyl group with reattachment of another water molecule would account for a constancy of active sites. Figure 5 is a possible mechanism proposed by them which is consistent with this sequence of events. The authors contend that the attack on carbon by this mechanism would lead to a honeycomb effect which would preserve the original bulk volume.

Carbon steam reactions at 1200°F were studied by Lewis, Gilliland, and Hipkin (17). Charcoal produced from wood and impregnated with K_2CO_3 was reacted with pure steam and mixtures of steam with carbon monoxide, carbon dioxide, hydrogen, and argon to determine the effect of low temperature operation on the reaction rate and mechanism. Adding 10 percent by weight K_2CO_3 to the charcoal sample yielded reaction rates at 1200°F that were 7 to 40 times higher than were previously extrapolated from data at temperatures of 1400° to 1800°F. Product gas compositions were essentially hydrogen and carbon dioxide, which supports the notion that the water gas shift reaction was always at equilibrium regardless of pressure or steam flow rate. The reactions involving solid carbon were observed to be below equilibrium.

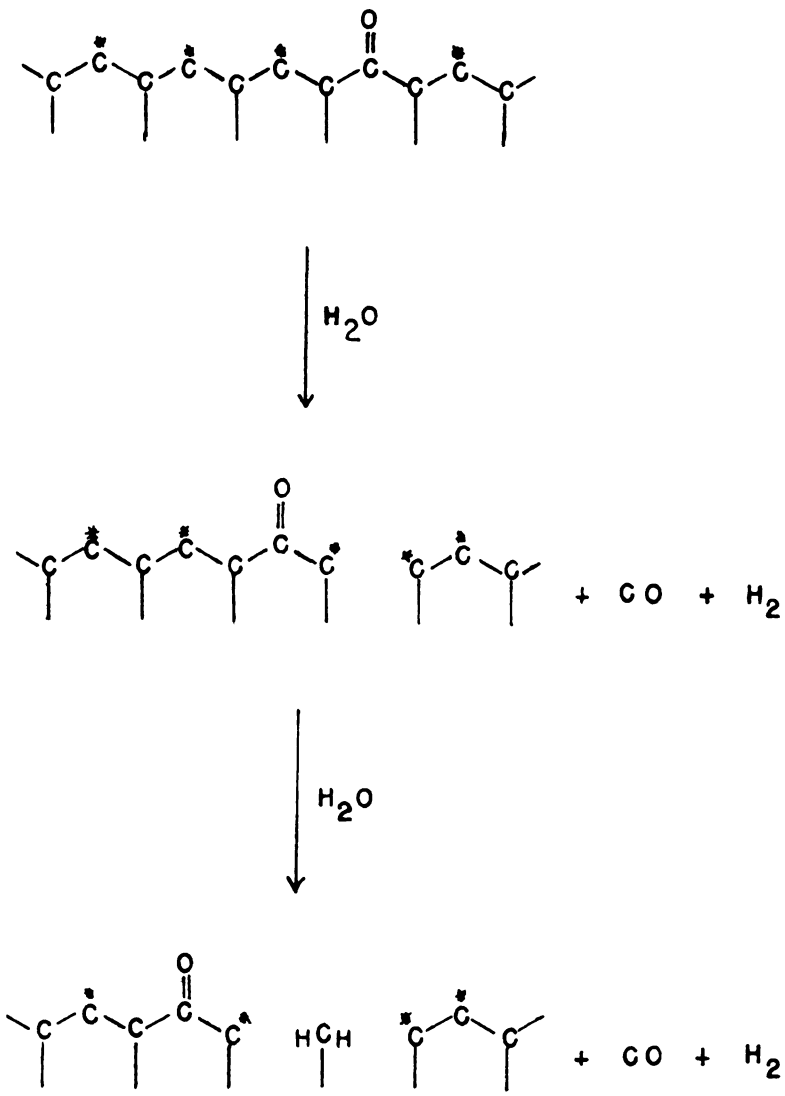

*Denotes active site.

Figure 5.--Reaction mechanism of char gasification.

Equation 6 is an empirical equation for which the catalyzed gasification rate was correlated. Partial pressures were measured at the exit of the reactor.

$$\text{Gasification Rate} = K \left(\frac{P_{H_2O}}{P_{CO}\ P_H}\right)^{0.6} \qquad (6)$$

It was stated that this equation applies for a constant amount of carbon in the bed. No value of K was given nor were units provided. Mention is made of the fact that carbon dioxide may exert a retarding effect on the gasification reaction, contrary to other investigators. The authors believe that carbon dioxide may exhibit control on the catalyst by competitive adsorbtion on the active reaction centers.

Sterm, Logiudice, and Heinemann (18) experimentally tested the technical feasibility of direct conversion of cellulosic material into synthesis gas. Feed materials were dropped continuously into a packed bed reactor at 1000°C. The effects of catalyst on pyrolysis and equilibration of gases was evaluated using steel wool as a hot surface. Sugar and wood sawdust were subjected to a high temperature short residence time reaction. The gases formed were forced through the bed by autogenic pressure. This procedure was compared to steam gasification of sugar

charcoal in terms of gas production and composition. Catalytic cracking of the primary pyrolysis products was essential to obtain the high yield of gases produced. Results of the experiment prove that 50/50 molar mixtures of CO and H_2 can be obtained by rapid high temperature pyrolysis of cellulosic material on a small scale if steel wool is used as a catalytic cracking material. Steam gasification yielded 4 to 8 percent CO_2 due to the water shift reaction. While results obtained using Alundum were erratic, two important observations were apparent: (a) gas compositions obtained over steel wool approach equilibrium since cracking occurs very rapidly, and (b) thermal decomposition of pyrolysis products over Alundum leads to kinetically controlled mixtures.

Walkup and researchers (20) have investigated gasification of biomass in the presence of multiple catalysts such as Na_2CO_3, K_2CO_3, and $Na_2B_4O_7 \cdot 10\ H_2O$. Preliminary experiments have demonstrated the following trends: (a) catalytic steam gasification appears promising using alkali type catalysts. K_2CO_3 gives the largest rate enhancement, while $Na_2B_4O_7 \cdot 10\ H_2O$ has the least activity of the chemicals studied, (b) increased gas production is due to less tar formation when an alkali carbonate catalyst is present, (c) catalyst impregnation

is better than dry mixing, and (d) H_2 production is enhanced at 500° to 650°C in the pressure of steam.

The thermochemical conversion of biomass will undoubtedly require a multitude of process studies, depending on the composition, physical structure, and size of the raw material. R. L. Garten (19) has presented a few positive aspects of biomass conversion. The first reason for the utilization of biomass as an energy resource is the very low sulfur content, 0.1 percent as compared to coal which is typically 2 to 3 percent sulfur. A second important aspect is the renewable nature of the material. He also mentions two negative characteristics of biomass. Due to its partially oxidized state, the energy content of biomass is low compared to coal. This is the reason for hydrogenation by steam, or by direct contact of H_2. The low bulk density also presents a problem, since a high degree of reactivity is necessary to reduce reactor size. The author also mentions that wood, owing to its structure, is expected to be easier to convert to fuel than coal.

The actual mechanism of the steam carbon gasification reaction is still unknown, particularly in the presence of alkali salts which may catalyze the gasification reaction, according to the previous investigators (16, 17, 18, 19, 20). Since the alkali salts may enhance

other simultaneous reactions, such as direct hydrogenation of carbon, the calculation of the gasification reaction rate may be complicated by the interpretation of the reactions occuring in the system. Besides affecting possible reaction pathways, a catalyst may also affect the adsorbtion/desorbtion process thereby entirely changing the reaction rate law dependence.

Early Pyrolysis and Gasification Experiments

The original objective of this work was to do experimentation and modeling of wood gasification. However, after a series of preliminary experiments and only qualitative results, the objectives were modified to study wood char gasification. These preliminary experiments were useful in gaining more experience with taking gas samples and handling the gas sampling procedure. Details of the study of wood char gasification are contained in a later section.

Uncatalyzed wood samples of approximately 5 to 7 grams, oven dried for 24 to 48 hours, were pyrolyzed in steam at temperatures ranging from 400° to 700°C. The pyrolyzing steam composition was always more than 95

percent steam with the remainder being nitrogen. Recordings of gas flow were made every 30 seconds, while gas compositions were monitored at approximately 3 to 4 minute intervals. The following observations were made based on 12 experiments. Six experiments involved nonimpregnated samples. Results are as follows:

A. Nonimpregnated samples

1. Smoke production begins within 30 seconds after insertion of the sample into the reactor at all temperatures. This may be explained by two factors. A thermal lag within the material leads to a time lag in the decomposition process as the temperature profile is developed, and secondly, there is a small lag due to the residence time of the product gases in the gas sampling train.

2. The highest rate of gas production is approached within approximately one minute for all temperatures. The maximum gas evolution occurs at a later time interval, which is a function of temperature. For 400°C the maximum occurs at 5 to 6 minutes, while at 700°C the peak occurs at 2 to 3 minutes.

3. Composition of the effluent gas varied from one run to the next due to errors in gas sampling. Approximate compositions which did not

appear to vary significantly with temperature were 45 percent CO and 45 percent CO_2, with the remaining 10 percent composed of varying amounts of H_2 and CH_4. CH_4 composition was highest near the beginning of the runs.

4. Solid residue remaining 15 to 17 minutes after insertion of the sample was approximately 15 percent of the original dry weight. Since all samples were oven dried before pyrolysis, weight loss due to desorption of water was negligible, and the total weight loss was a reproducible quantity. The char retained the original fibrous structure even after 85 percent weight loss. All uncatalyzed samples reacted in a steam environment at 700°C lost 85.6 percent weight as volatile gases and tars. Therefore, high temperature reaction of dried wood with steam is essentially pyrolysis up to about 85 percent weight loss. Results of weight loss measurements were the same in steam and nitrogen environments.

B. Salt impregnated samples

Pyrolysis by steam of wood impregnated with 12 percent by weight of K_2CO_3, produced results significantly different than similar uncatalyzed runs. The pyrolysis steam mixture was again 95 percent

steam and the remaining 5 percent nitrogen. Gas flow measurements were made every 30 seconds, while gas samples were taken every 3 to 4 minutes. Gas composition measurements were significantly improved due to increased experience. The following details distinguish the results between catalyzed and noncatalyzed runs.

1. Smoke production occurs much earlier and is less dense than observed for noncatalyzed runs. Most of the smoke evolution was over in 30 seconds.

2. Gas production curves peak earlier than noncatalyzed runs. Gas production rates versus reaction time are plotted in Figure 6 for preliminary catalytic runs for three temperatures.

3. The increased hydrogen composition indicates that gasification is occuring in addition to pyrolysis. CO_2 varies from 27 to 30 percent over the temperature range, while H_2 varies from 52 to 67 percent. CO is less than 1 percent for nearly all the gas samples analyzed. CH_4 was negligible.

4. The most significant observed difference between the catalyzed and uncatalyzed runs was the nature of the structure of the remaining ungasified

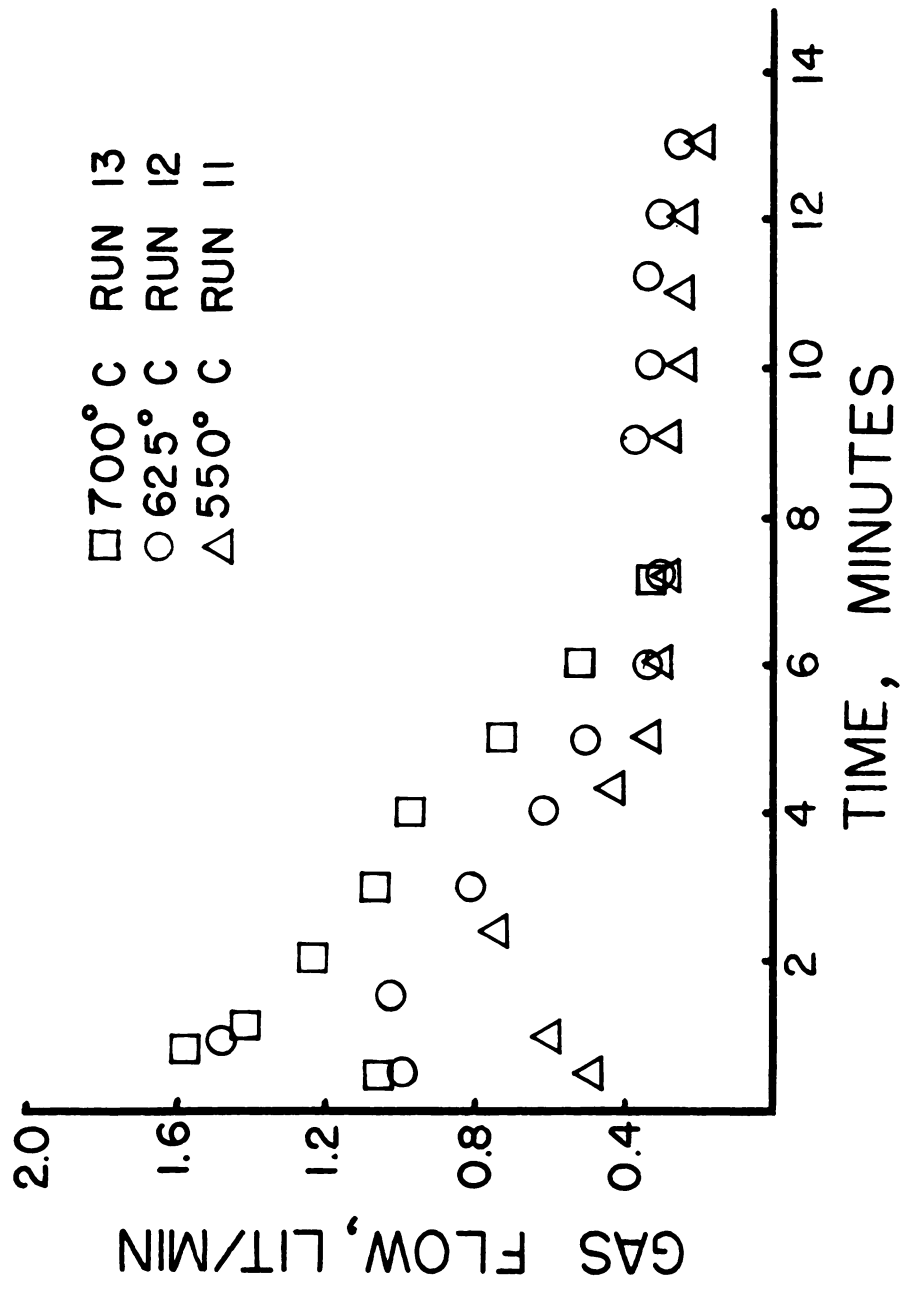

Figure 6.--Observed gas flow from pyrolysis of K_2CO_3 impregnated wood.

material. No microphotographs were taken, but it appeared as though no original fibrous wood structure remained after the initial reaction period for the catalyzed samples. The remaining char is a highly porous and brittle material, which appeared to have had some foaming action occuring during pyrolysis. Some of the sample had become encrusted on the exterior of the sample basket in the reactor.

5. For runs 12 and 13, which were performed at temperatures of 625° and 700°C, respectively, nearly all of the char was consumed. The remaining material was highly porous and brittle. A small amount in water produced a basic solution. It appeared to be some form of potassium oxide.

Experimental data on simultaneous pyrolysis and gasification of wood is difficult to analyze. Some quantitative information on product gas composition and gas production flow rates was obtained, however smoke and tar production were not determined quantitatively. The original objective of this study of the gasification of the wood, was redefined to overcome problems related to production of tars and other liquid products which could not be determined quantitatively and plugged the reactor

exit several times. Also some products, CO and CO_2, were common to both pyrolysis of raw wood and gasification, thus interpretations of results were complicated. For these reasons gasification of pyrolyzed wood char was investigated.

EXPERIMENTAL CONDITIONS

Introduction

Char samples were prepared from dried samples of Poplar SPP. Char samples were impregnated with Na_2CO_3 and K_2CO_3 and gasified at various temperatures, steam partial pressures, and space velocities. The following range of experimental conditions were used to study the kinetics of pyrolysis and gasification of char: (a) steam partial pressure of 45 to 100 kPa, (b) space velocity range of 2 to 7.25 sec^{-1}, and (c) temperature range of 500° to 700°C. These experiments were conducted in a differential fixed bed reactor. Small sample size of 1 to 2 mm in diameter was chosen to maintain temperature and concentration gradients to a minimum. High gas velocities of 10 to 35 cm per second were chosen to minimize reaction of product gases with the reacting char due to the short contact times involved. By observing gas flow, gas composition, temperature, and total sample weight loss, evaluation of the kinetic parameters for the system was accomplished. Additional information was also observed on the effects of 12 percent by weight of Na_2CO_3 and K_2CO_3 on the gasification rates.

Reactant Gas Production

Figure 7 is a schematic diagram of the reactor system. A large water reservoir (A) is suspended six feet over the reactor assembly. A needle valve provides a constant supply of feed water between 0 and 12 cm^3 per minute and is mixed with a set flow of nitrogen. The nitrogen is controlled by a tank regulator, valve, and flow meter arrangement (C). Combined nitrogen and water stream is then fed to a vaporizing furnace (E), where water is vaporized and the gases are heated to high temperatures before entering the reactor. The water and nitrogen stream is heated in the gas fired furnace by flowing through a stainless steel cylinder (D) 130 mm long and 51 mm in diameter, with combustion gases impinging on the outside. The hot gases flow out of a vaporizing heater into a 6.35 mm O.D. heavily insulated stainless steel tube that delivers the hot gas mixture to the reactor (H). Temperature control of the reactant gas is accomplished by adjustment of the furnace flame and the flow rates of nitrogen and water. The temperature of the reactor system was allowed to stabilize for approximately 10 to 15 minutes before making a run. Gas temperatures between 400° to 800°C were obtained for steam partial pressures between 45 and 100 kPa and reactor space velocities of 2 to 7.25 sec^{-1}.

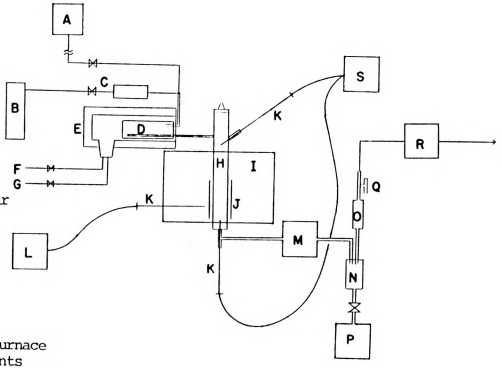

(A) Water Supply Reservoir
(B) Nitrogen Cylinder
(C) Nitrogen Valve and Flowmeter
(D) Gas Preheater
(E) Preheater Furnace
(F) Air Line
(G) Natural Gas Line
(H) Inlet to Reactor
(I) Heavy-Duty Electric Furnace
(J) Furnace Heating Elements
(K) Chromel-Alumel Thermocouples
(L) Wheelco Temperature Controller
(M) Condenser
(N) Constant Level Reservoir
(O) Drierite Column
(P) Condensate Collection Vessel
(Q) Gas Sampling System
(R) Wet Test Meter
(S) Leeds and Northrup Potentiometer

Figure 7.--Schematic of experimental apparatus.

Reactor Assembly

The reactor assembly, Figures 8 and 9, is constructed entirely of type 304 stainless steel. The reactor tube (H) is 336.5 mm in length and 44.5 mm O.D., and 38.1 mm I.D. is placed within the heavy-duty electric furnace (I) such that the bottom 100 mm of the tube are heated by means of the furnace heating elements (J). Furnace capacity ranges up to 560 watts.

Temperature is monitored by means of three chromel-alumel thermocouples (K). One thermocouple is centered in the reactor cavity 75 mm above the heating zone of the reactor to monitor the incoming gas temperatures. This thermocouple is removable to facilitate addition and removal of the sample. The second thermocouple is located at the bottom of the sample compartment (i.e., the heating zone) to provide data on the sample and exit gas temperatures. Both thermocouples are mounted by welded 6.35 mm O.D. stainless tubing and Swaglok fittings. A third thermocouple is situated near the heating elements of the electric furnace to provide a temperature signal for a Wheelco temperature controller (L).

The top of the reactor is removable by a spring arm arrangement to provide rapid manual sample addition and withdrawal. Asbestos is used as a seal between the top of the reactor and the reactor cap.

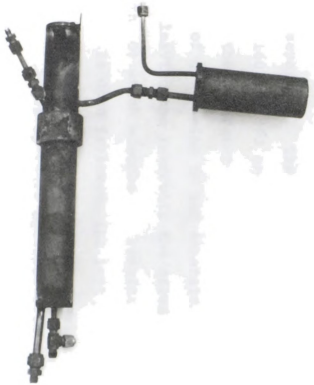

Figure 8.--Picture of reactor assembly showing main reactor tube and steam preheater.

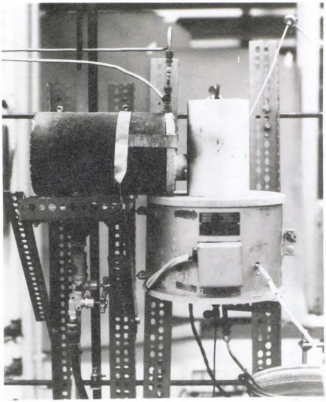

Figure 9.--Picture of reactor assembly.

A 100 mm long by 36 mm O.D. stainless steel screen basket fits snugly into the reactor to serve as a sample holder. This is raised and lowered into place to initiate and terminate the run, respectively.

Product Gas Processing

Product gases exit the reactor and flow into a water immersed copper coil (M) which cools the gases to approximately 20°C, and condenses any nonvolatile products and water vapor in the product stream. Liquid water separation is accomplished in a small vessel of 50 cm^3 in volume (N). The liquid level was maintained approximately half full. The liquid was continuously drained into a beaker at a rate which would maintain a constant level in the separator. The total volumetric flow of gas ranged between 160 and 500 cm^3 per minute, thus the gas residence time in the separator was less than 0.1 seconds. The effect of gas mixing in the separator was neglected. After leaving the reservoir the gases flow into a Drierite column (O) which adsorbs any remaining water. Gas sampling is done following the last water removal step (Q). Gas sampling was accomplished using 2 cm^3 capacity Pressure-Lok gas syringes equipped with side port needles and valves. Based on calculations using the calibration data, accuracy with 0.5 cm^3 samples was within 5 volume

percent. After gas sampling product gases then pass continuously through a Precision wet test meter (R) which is used to measure the flow rate and total gas production with time.

Additional equipment required for the experimental apparatus included a Wheelco pyrometer (L) for furnace temperature control, Leeds and Northrup potentiometer (S) for monitoring the reactor temperature via chromel-alumel thermocouples, and a Perkin-Elmer model 154 Vapor Fractometer with accompanying Photovolt 43 strip chart recorder.

Gas Analysis

Syringes were used to take 2.0 cm^3 aliquots of gas periodically during a run, and the gas samples were later analyzed with a Perkin-Elmer model 154 Vapor Fractometer. In order to flush the needle and valve assembly, 1.5 cm^3 of the sample was purged into the atmosphere, and the remaining 0.5 cm^3 was injected into the chromatograph column. This procedure was utilized to reduce possible contamination due to the other gases in the needle. The packing material used in the column is carbosieve S 100/120 mesh. Glass column dimensions are, 1830 mm in length by 6.35 mm O.D. with an I.D. of 3.175 mm (6 ft. x .25 in O.D. x 0.125 in I.D.). A thermal conductivity detector provides adequate response for all the gases analyzed,

provided neon is used as a carrier gas. It is especially important to note that using helium as a carrier gas does not allow sufficient sensitivity to hydrogen. A column temperature of 136°C and 15 cm^3 per minute of neon flow provided an adequate retention time for the required peak separation. Calibration was achieved by separate analysis of pure 0.5 cm^3 samples of each of the component gases. Response of hydrogen was assumed linear over the concentration range observed.

Sample Preparation

For pyrolysis experiments Poplar SPP was ground in a hammer mill then oven dried and stored in a dessicator. For the salt impregnated experiments the wood was pretreated with 12 percent Na_2CO_3 and K_2CO_3 solutions, then oven dried. Average particle size was 1 mm in diameter and 2 to 4 mm in length. No change in size was obtained after salt pretreatment. Sample sizes for the pyrolysis experiments ranged between 5 and 7 grams.

For all the gasification experiments the finely divided wood was pyrolyzed at 700°C in flowing nitrogen for 10 minutes. The pyrolysis time of 10 minutes was based on previous observations that no additional weight loss of wood was observed after 5 minutes at those conditions. Char gasification sample sizes were 2.67 grams

(±0.03 grams), except in the case of the salt impregnated char, for which the total carbon content of the sample was approximately 2.67 grams. Total sample weight for these runs are higher due to the added weight of the alkali salt. All samples are thoroughly dry before use.

Operating Procedure

The char addition which initiates the run was begun after the system had been maintained at the desired operating temperature and flow conditions. Correct operating conditions were achieved when temperature readings from thermocouples above and below the sample chamber were equal, and constant water and nitrogen flow rates were observed. At this time the wet test meter was zeroed and the top of the reactor removed. The sample was quickly inserted into the reactor and the reactor cap and condensate vessel were simultaneously put in place. The beginning of the reaction sequence required a total time of three seconds. Conditions were maintained constant over the 5 to 10 minute period of the run, during which three to five gas samples were taken usually three minutes apart. The temperature of the reaction environment was monitored during the reaction as was the gas flow rate with time. Since analysis time for each gas sample is 12 minutes, part of the gas analysis was completed

after the run had ended. All gas samples were analyzed within one hour.

EXPERIMENTAL RESULTS

Effects of Pyrolysis

A microphotograph of Poplar SPP is shown in Figure 10. From this photograph it can be seen that the structure is quite regular and that there are essentially two sizes of pores, the vessels were measured to be 70 μm in diameter while smaller tracheids were measured to be 20 μm in diameter. The cellular structure has cell walls of 2 to 4 μm in thickness. Details of the aforementioned cellular structure as described in Figures 1 and 2 are apparent, particularly the large S2 layer which comprises a majority of the cell wall. The highly porous nature of the wood is readily apparent.

A series of electromicrophotographs were taken of wood after having been exposed to a high temperature gasification environment. Three millimeter diameter samples were pyrolyzed in 600°C steam for periods of 1, 4, and 8 minutes, and electromicrophotographs of these samples are shown in Figure 11, 12, and 13, respectively. Photographs of the material after just one minute of exposure shows two striking morphological changes. It can be seen that there is a slight reduction in size of the tracheids and

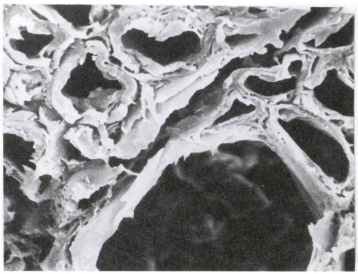

Figure 10.--Electrophotograph of Poplar SPP.

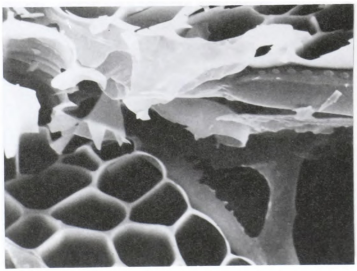

Figure 11.--Electromicrophotograph of Poplar SPP after 1 minute of pyrolysis.

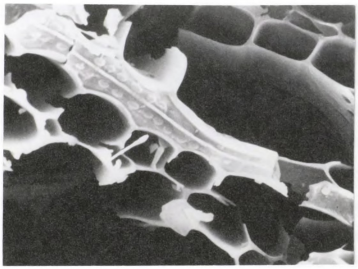

Figure 12.--Electromicrophotograph of Poplar SPP after 4 minutes of pyrolysis.

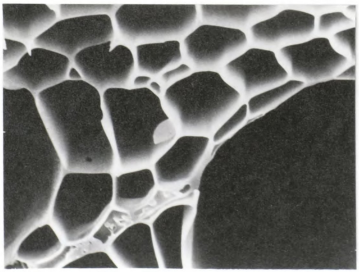

Figure 13.--Electromicrophotograph of Poplar SPF after 8 minutes of pyrolysis.

enlargement of the vessels. Secondly, a reduction occurs in the thickness of the individual cell walls. After one minute of gasification, the cell walls are reduced to 0.5 to 0.8 μm in thickness, corresponding to an 80 percent loss in size. Weight loss measurements for the samples indicate 85 percent weight loss after 8 minutes of gasification. Therefore the initial density of the cell walls of the unpyrolyzed wood of 1.5 grams per cm^3 remains essentially constant during pyrolysis while the apparent bulk density of the char particles becomes 0.06 grams per cm^3. The cell walls of the residual material appear to be uniform in structure, with fragile cellular components remaining quite intact. There is no apparent fissuring or cracking of the cell walls except in the areas adjacent to the vessels, and they appear to remain quite impermeable, despite the fact that 85 percent weight loss has occured. Photographs of the samples exposed to the same high temperature for periods of 4 and 8 minutes appear very similar to the photographs after one minute of gasification.

These observations indicate that during the early periods of gasification and pyrolysis of wood, the fine structure of the cell walls is decomposed where as the macropore structure of the solid residue is essentially the same as the macropore structure of the original dried wood before reaction.

Salt Catalyzed Wood Char Gasification

The experimental work was done jointly with Mr. Craig Anderson. Experiments were done on both salt impregnated and nonimpregnated wood char samples. Results of the nonimpregnated experiments are reported in detail in Mr. Anderson's thesis. This thesis reports details of gasification experiments for salt impregnated wood char and comparisons are made with results of experiments on nonimpregnated samples. Reaction conditions and techniques were duplicated for the catalytic and noncatalytic runs. Table 3 contains a summary of experimental conditions and results.

The catalytic activities of two different salts, Na_2CO_3 and K_2CO_3 were investigated. These salts were chosen since they have been shown (20) to be effective in reducing tar formation in pyrolysis and the enhancement of gasification. Details of the preparation of the salt impregnated samples are presented in the experimental section. Samples contain approximately 12 percent by weight. Ten experiments were conducted for partial pressures of steam between 45 and 100 kPa for each catalyst, temperatures of the reaction environment of 550°, 625°, and 700°C for each catalyst, and all at a space velocity of 4 s^{-1}.

Gasification reaction rates were calculated for each run based on two different assumptions. In case A, it is assumed that methane is produced by direct hydrogenation of char, thus the reaction rate of char gasified is proportional to the rate of production of carbon oxides, whereas in case B it is assumed that methane is produced by reaction of carbon monoxide and hydrogen, thus the rate of char gasified is proportional to the sum of the rates of carbon oxides and methane. Therefore reaction rates were calculated for each run based on (a) total production of CO and CO_2 in the effluent, and (b) total production of CO, CO_2, and CH_4. See Appendix B for sample calculation of reaction rate.

Carbon monoxide is the direct result of gasification.

$$C\ (s) + H_2O\ (g) \longrightarrow CO\ (g) + H_2\ (g) \qquad (7)$$

But due to high temperature and high concentration of steam in the system, the shift reaction also takes place.

$$CO\ (g) + H_2O\ (g) \longrightarrow CO_2\ (g) + H_2\ (g) \qquad (8)$$

Previous workers have usually considered the shift reaction to be fast and thus always in equilibrium. Due to stoichiometry the total moles of carbon oxides in the effluent

stream will not change, and will be equal to the total moles of CO formed from the gasification reaction. Three other reactions are important at the experimental conditions.

$$C\ (s) + CO_2\ (g) \longrightarrow 2\ CO\ (g) \qquad (9)$$

$$C\ (s) + 2\ H_2\ (g) \longrightarrow CH_4\ (g) \qquad (10)$$

$$CO\ (g) + 3\ H_2\ (g) \longrightarrow CH_4\ (g) + H_2O\ (g) \qquad (11)$$

Reaction 9 is the Boudouard reaction and occurs at a very slow rate at experimental temperatures. Reaction 10 is favored by equilibrium at low temperatures. The other possibility of methane formation within the system is reaction 11. If reaction 11 is the source of methane in the product gas, then the total moles of methane should be included in the determination of the reaction rate. Due to stoichiometry, the total moles of methane formed by reaction 11 is equal to the moles of carbon monoxide consumed.

Depending upon the source of methane, the rate may be calculated in two different manners. Assuming reaction 11 is occurring, then the production of methane must be included in calculating the rate of gasification. If the source of methane is carbon, perhaps by catalyzed direct

hydrogenation, then methane must be neglected in calculating the rate. Both cases are considered in the following steam partial pressure experiments.

To evaluate the affect on steam concentration of the reaction rate, the space velocity was maintained at 4 s^{-1} and reaction temperature was held constant at 625°C, while steam partial pressure was varied from 45 to 100 kPa. Figure 14 is a plot of experimental results assuming methane to be produced by direct hydrogenation of char. Due to scatter of the experimental points it is difficult to determine the reaction order with respect to steam with much precision. As can be seen in Figure 14 a first order in steam rate equation is appropriate for both uncatalyzed and catalyzed material. Figure 14 is a plot of experimental results assuming methane to be produced from carbon monoxide and hydrogen reacting. Comparison of Figures 14 and 15 indicates for Na_2CO_3 catalyzed runs there appears to be no appreciable difference in methods for treating the data, since methane production was quite small. K_2CO_3 catalyzed char exhibits higher reaction rates since the methane product gas contributions were high for these runs, but the data still appears roughly first order. It is apparent that first order kinetics for the gasification reaction are consistent with both methods for treating the data for both salts.

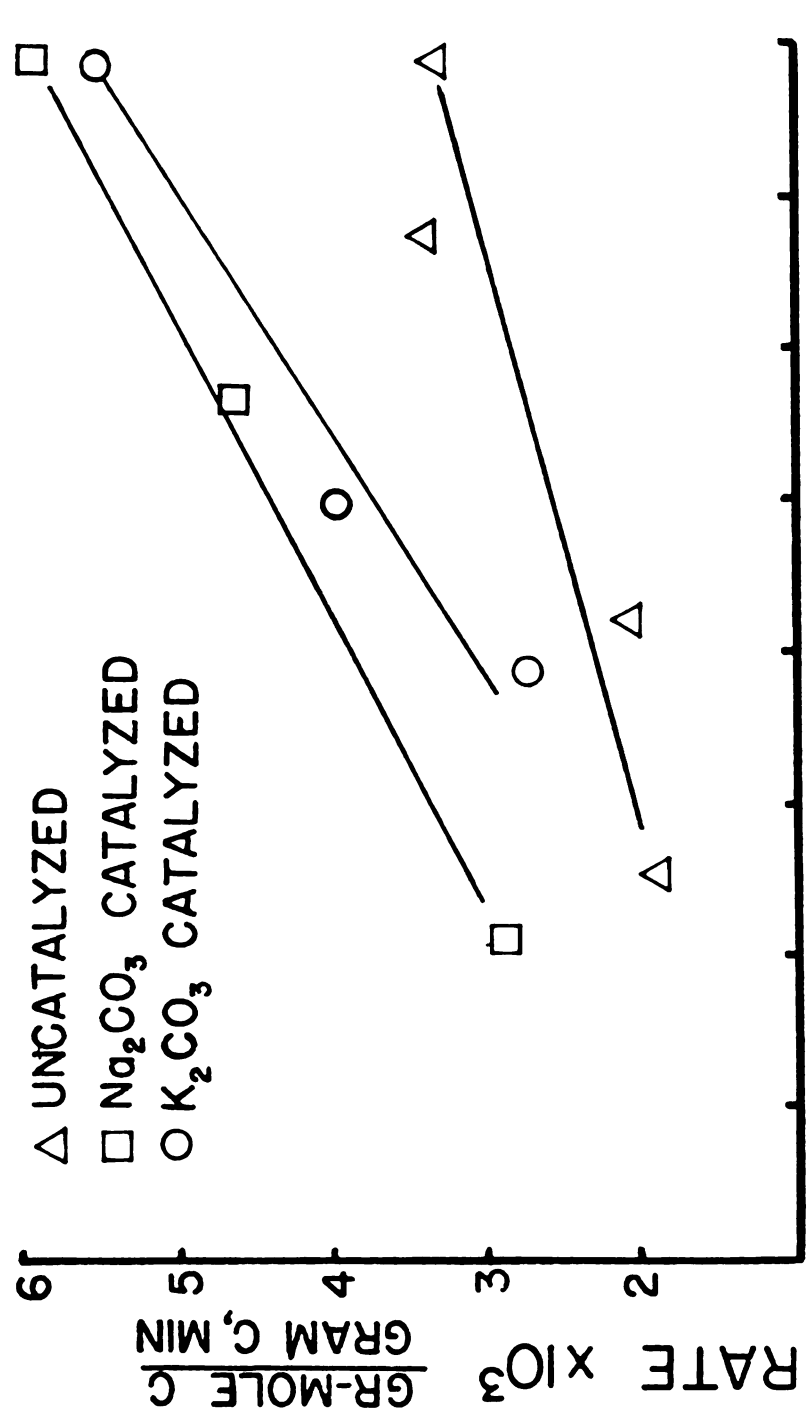

Figure 14.--Effect of steam partial pressure on reaction rate calculated from CO and CO_2, Case A.

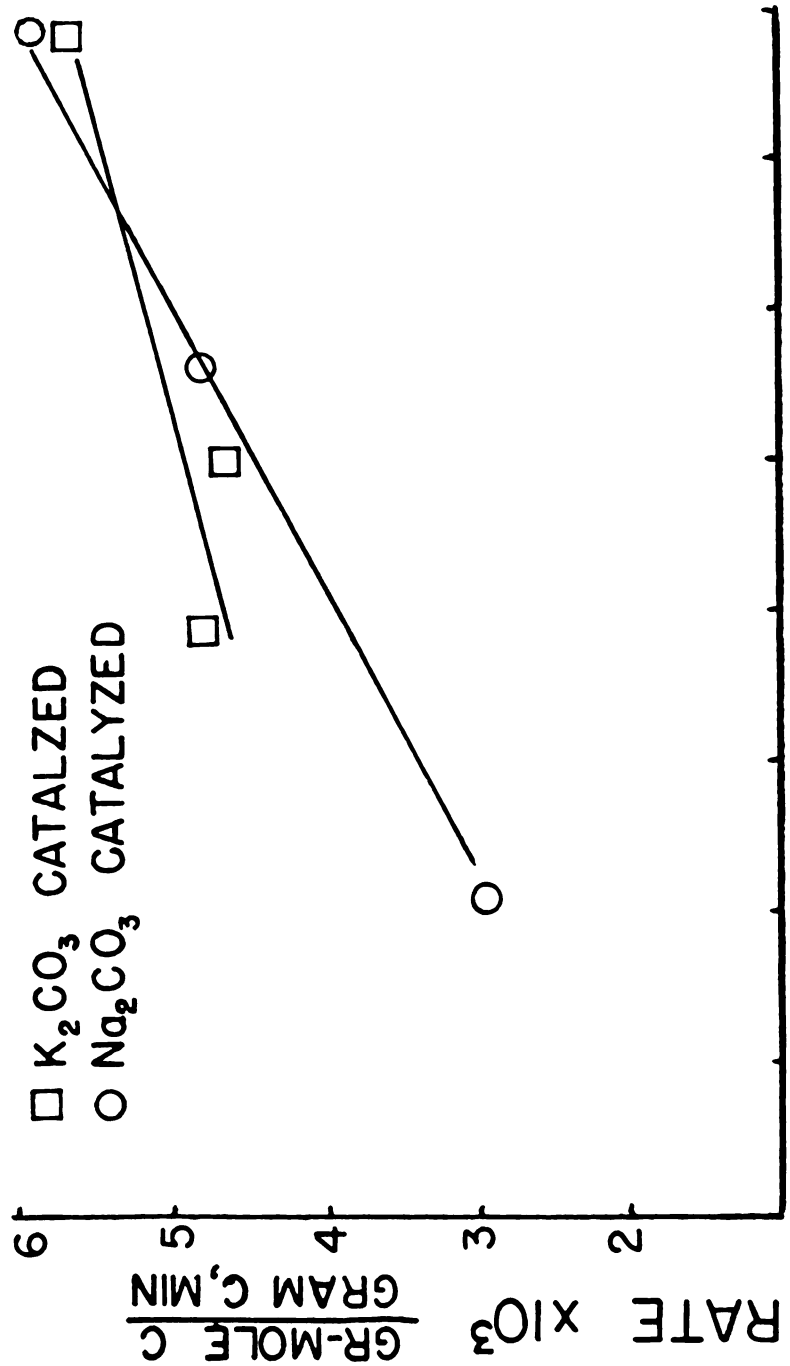

Figure 15.--Effect of steam partial pressure on reaction rate calculated from CO, CO_2, and CH_4, Case B.

The following equation is suggested for the rate of gasification.

$$\text{Gasification rate} = k(T)\ p_{H_2O}\ \frac{\text{moles reacted}}{\text{gr C, minute}} \qquad (12)$$

Activity of char is assumed to be unity, therefore it does not appear in the rate expression.

These results are in contrast to the results for the noncatalyzed experiments, where it appears that Langmuir-Hinshelwood kinetics fit the data well for case B methodology.

Assuming a typical Arrhenius dependence on the rate constant, activation energies were calculated. This was accomplished by determining the reaction rate versus the inverse of the absolute temperature for 550°, 625°, and 700°C, see Figure 16. The resulting activation energy for Na_2CO_3 is 84.9 kJ/mole, while that of K_2CO_3 is 94.2 kJ/mole. Uncatalyzed char had an observed activation energy of 157 kJ/mole. Assuming a first order reaction rate and an Arrhenius temperature dependence, frequency factors were calculated and then averaged. Average values were then used for calculated reaction rates. Averaged frequency factors found were 10.7 and 16.4 moles/gr C minute kPa for Na_2CO_3 and K_2CO_3, respectively. All rate data are summarized in Table 3 in the Appendix.

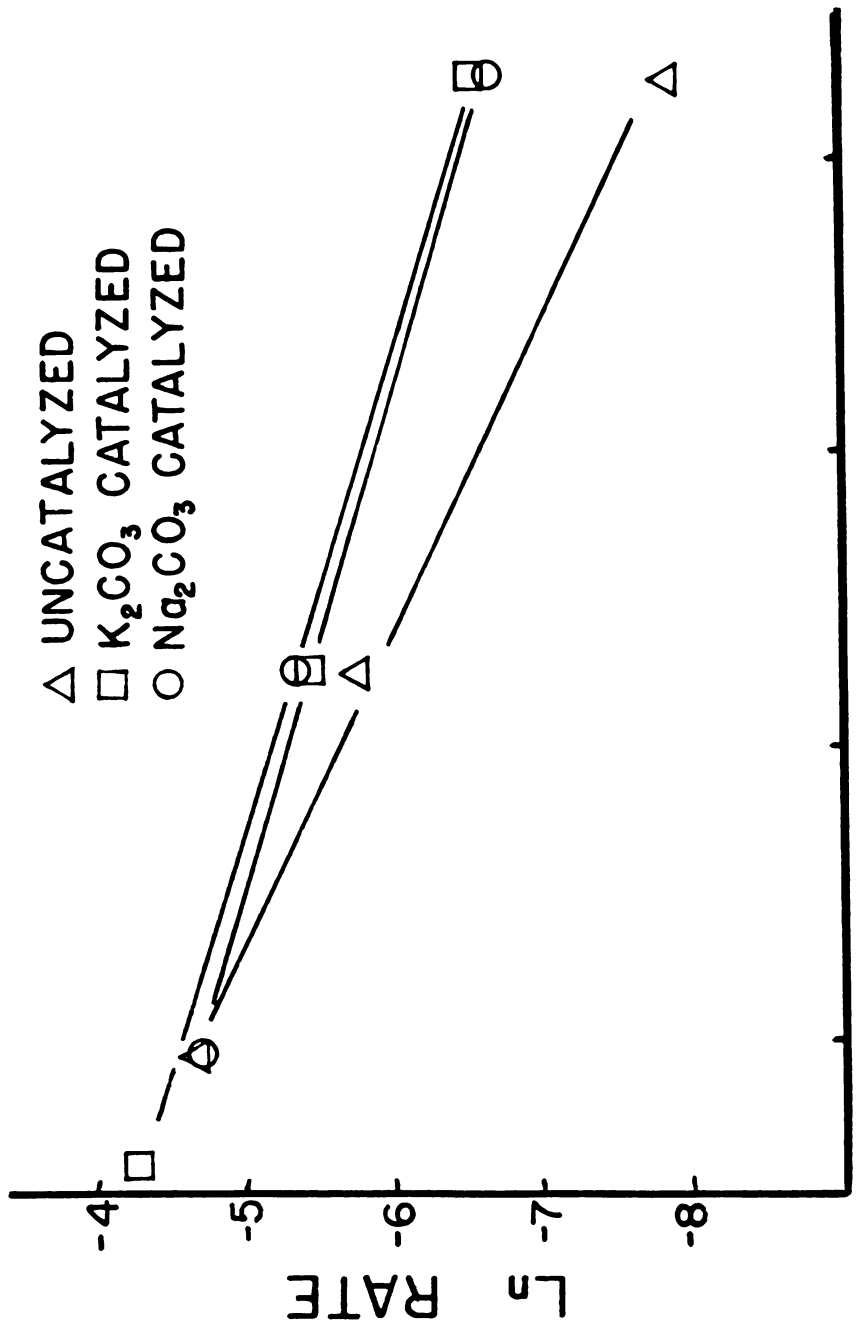

Figure 16.--Activation energy plot, ln rate versus I/T.

Space velocities of 2, 4, and 7.25 seconds $^{-1}$, based on 99 percent steam and the volume of the sample basket, were obtained in experiments performed on noncatalytic samples at 625°C because the reaction rate was most accurately observable at that temperature. Pure steam was used for all these runs. Results are presented in Figure 17. No significant change was observed between the space velocities of 2 and 4 sec^{-1}, where as the reaction rate dropped by about 25 percent at a space velocity of 7.25 sec^{-1}. The observed behavior is opposite to that expected for increasing gas flow. This observation has been difficult to interpret. If the data are correct, then one could account for the observed behavior by assuming a negative order reaction rate with respect to steam. An increase in space velocity would increase the external steam concentration thereby reducing the overall rate. Since a negative reaction rate dependence is contrary to the experimental data on steam partial pressure, the deviation must be the result of experimental error, either in the gas flow or temperature measurement. Since the data on gas flow and composition is otherwise consistent, it seems improbable that either is the source of error. An increase of heat transfer from the gas to the thermocouple at higher space velocities may produce a more accurate temperature reading than that observed at

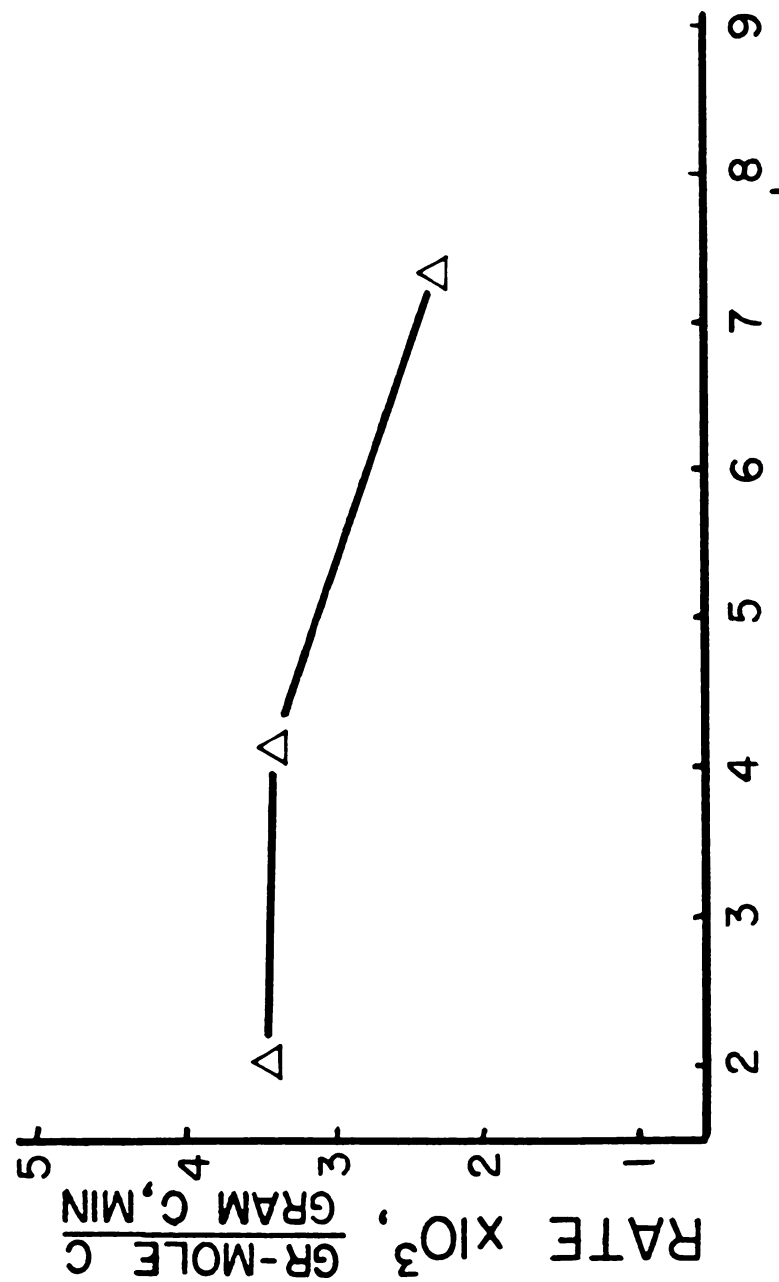

Figure 17.--Effect of space velocity in reaction rate at 625°C for uncatalyzed material only.

slower gas velocities. This is the most plausible explanation for the observed experimental behavior.

MODELING

Single Particle Effectiveness Factor

The observed intrinsic kinetic information has been combined with estimated diffusion coefficients to model a reacting particle. Figure 18 is a schematic diagram of the reacting particle. A flat slab geometry is justified by observations of pyrolyzed wood that indicate the original structure of parallel closely packed cells is retained in the char. The high impermeability of the cell walls is the justification for assuming one dimensional transport within the particle. Effective diffusivity within the particle has been calculated based on the Random Pore Model (25), Equation 13.

$$\frac{1}{\mathcal{D}_e} = \frac{1}{\mathcal{D}_{AB}} + \frac{1}{\mathcal{D}_K} \qquad (13)$$

where $\mathcal{D}_e$ = Effective diffusivity

$\mathcal{D}_{AB}$ = Bulk diffusivity

$\mathcal{D}_K$ = Knudsen diffusivity

The ratio of the pore diameter to the mean free path of steam at 700°C is over 100. This is a sufficient

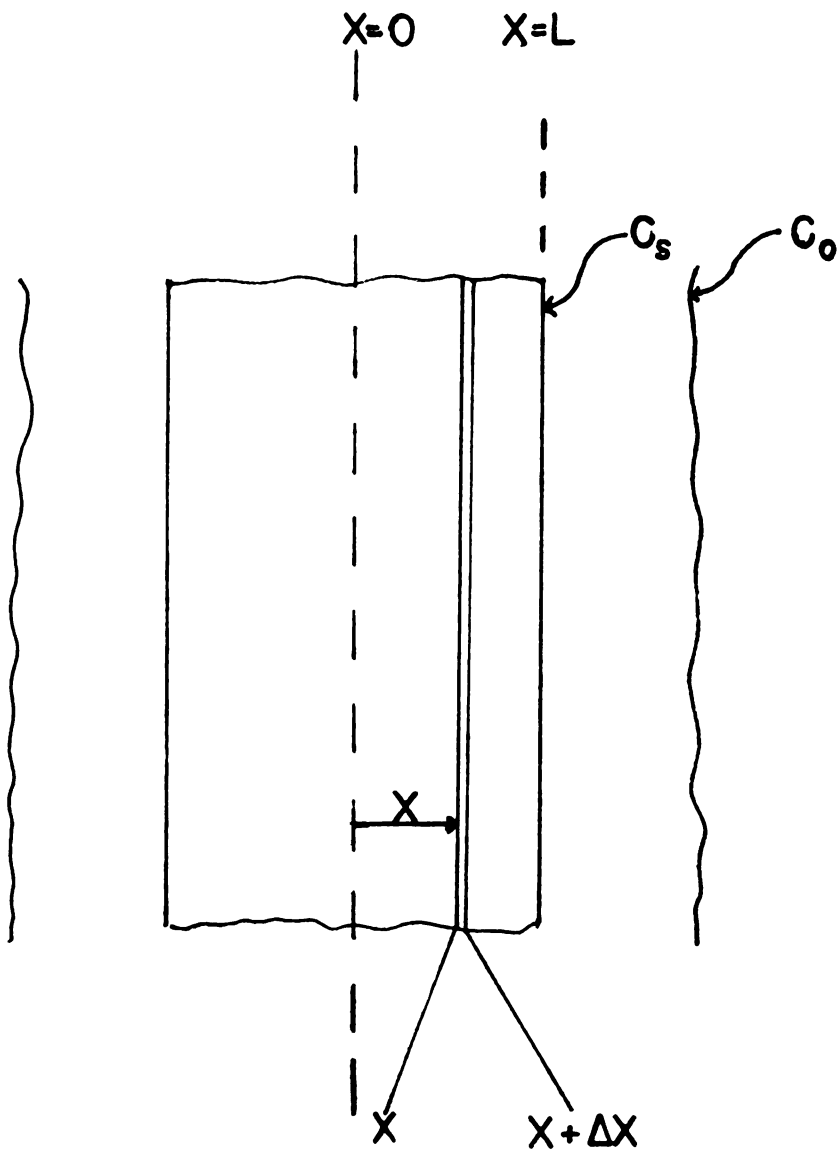

Figure 18.--Drawing of flat slab geometry for a particle with external bulk film resistance.

condition for neglecting the contribution of Knudsen Diffusion. $\mathcal{D}_{AB}$ was calculated from Equation 14.

$$\mathcal{D}_{AB} = D_{AB}\,\varepsilon^2 \tag{14}$$

where $\mathcal{D}_{AB}$ = Effective bulk diffusivity

D_{AB} = Bulk diffusivity

ε = Void fraction

A void fraction of 0.7 was calculated for the residual char. A bulk diffusion coeffecient for steam in the reacting mixture can be calculated using Equation 15.

$$D_{H_2O,\ \text{mixture}} = (1 - Y_{H_2O}) / \sum_{j=1}^{n} (Y_j / D_{j,\ H_2O}) \tag{15}$$

where Y_{H_2O} = mole fraction of steam

Y_j = mole fraction of the other species in the reacting mixture

Experimental binary diffusion coefficients for Equation 15 were extrapolated to higher temperatures using the Chapman Enskog formula. Using first order kinetics and a mass balance on the geometry in Figure 18, we have

$$\mathcal{D}_e \frac{\partial^2 C}{\partial x^2} = kC \tag{16}$$

$$\text{using } \psi = \frac{C}{C_o},\ \xi = \frac{x}{L}.$$

Equation 16 in dimensionless variables becomes,

$$\frac{\partial \psi}{\partial \xi} = \frac{L^2 k}{\mathcal{D}_e} \psi = \phi \psi \tag{17}$$

$$\text{where } \phi^2 = \frac{L^2 k}{\mathcal{D}_e}$$

The boundary condition at the center of the particle is

$$\frac{\partial \psi}{\partial \xi} = 0, \ \xi = 0 \tag{18}$$

while the boundary condition at the surface becomes

$$\frac{\partial \psi}{\partial \xi} = Bi_m \ (1 - \psi), \ \xi = 1 \tag{19}$$

for mass transfer through a stagnant boundary layer. Solving the differention Equation 17 with the boundary conditions 18 and 19, yields

$$\psi = \frac{\cosh \phi}{\frac{\phi \sinh \phi}{Bi_m} + \cosh \phi} \tag{20}$$

Effectiveness factor is defined as follows,

$$\eta = \frac{\text{rate observed}}{\text{rate } (C_o)} \tag{21}$$

$$\text{where } C_o = \text{bulk concentration}$$

and for this problem (see Appendix C),

$$\eta = \frac{\tanh \phi}{\phi \left(1 + \frac{\phi \tanh \phi}{Bi_m}\right)} \tag{22}$$

therefore

$$\text{Global rate} = \text{Intrinsic rate at bulk conditions} \frac{\tanh \phi}{\phi \left(1 + \frac{\phi \tanh \phi}{Bi_m}\right)} \tag{23}$$

The influence of particle size and finite external mass transfer rate on the isothermal effectiveness factor for the catalyzed reaction rate is shown in Figure 19. A value of $k = 1.519\ s^{-1}$ (Na_2CO_3 catalyzed gasification reaction rate at 625°C) was used for the isothermal effectiveness factor calculations. It can be seen that mass transfer becomes a significant factor for particles larger than 1.0 cm. This substantiates the fact that intrinsic kinetics were observed in the study, since experimental particle size was less than 0.3 cm. Figure 20 illustrates a comparison of effectiveness factor for catalyzed and uncatalyzed char at 625°C over a range of particle sizes. This result shows that diffusional resistances are more significant at higher reaction rates.

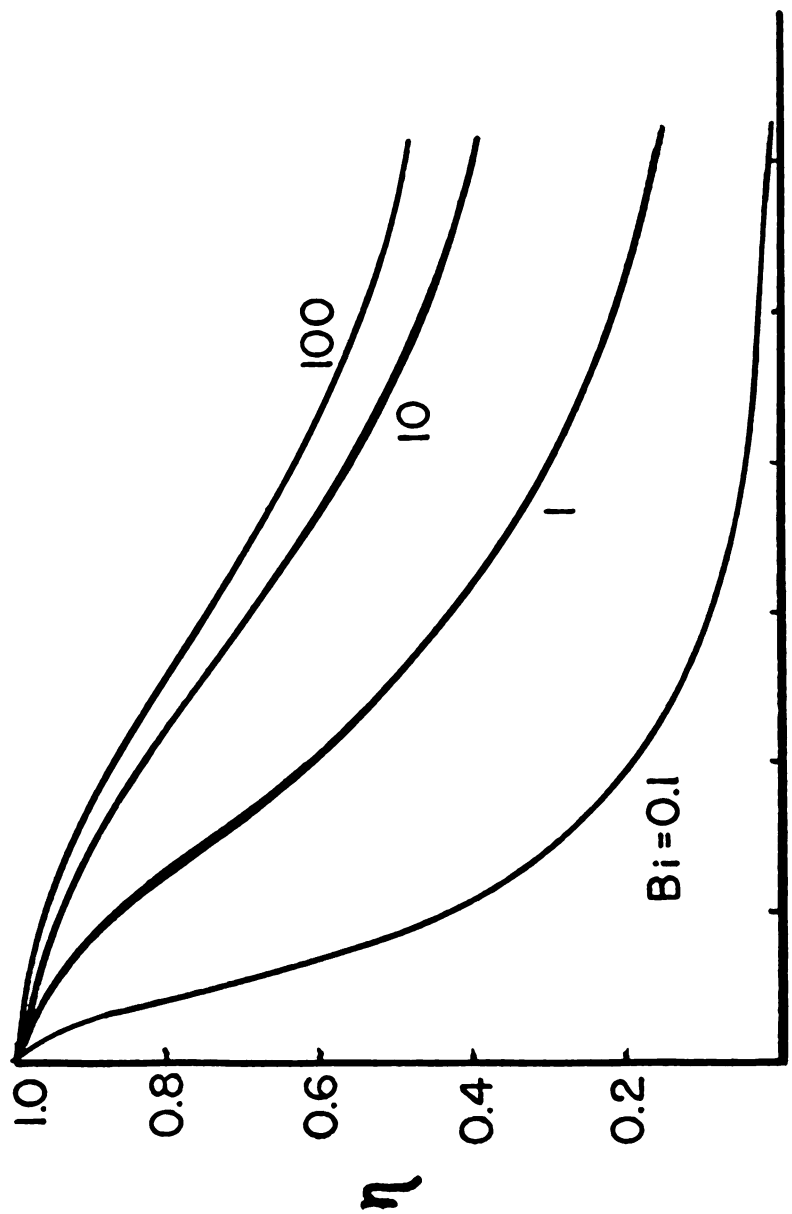

Figure 19.--Plot of effectiveness factor versus particle size, k = 1.519 s^{-1}, $\mathcal{D}_e$ = 3.19 cm^2/s.

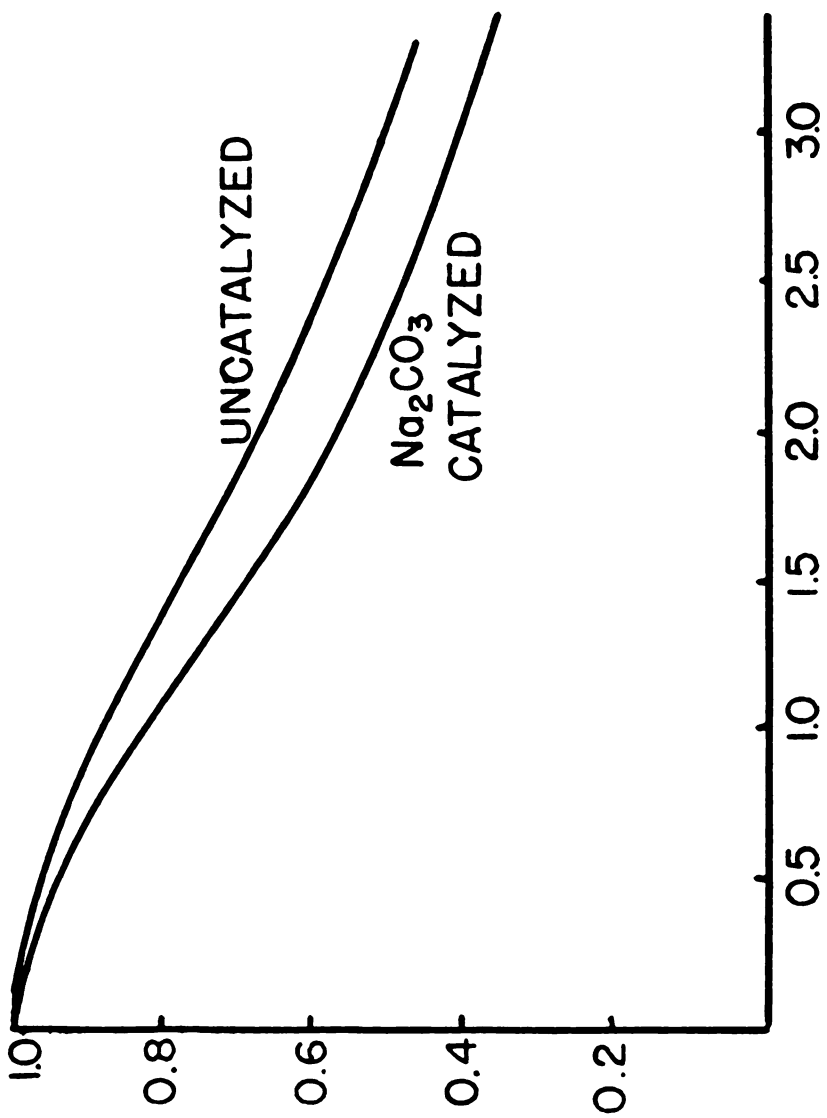

Figure 20.--Comparison of effectiveness factor for catalyzed ($k = 1.519\ s^{-1}$) and uncatalyzed ($1.14\ s^{-1}$) char, $\mathcal{D}_e = 3.19\ cm^2/s$.

Tubular Reactor Axial Dispersion Model

Considering an axial dispersion model for a tubular flow reactor, containing wood particles a mass balance for first order kinetics over a differential element as shown in Figure 21 yields

$$D_z \frac{\partial^2 C}{\partial z^2} - v \frac{\partial C}{\partial z} - \eta k C = 0. \qquad (24)$$

Defining the dimensionless variables,

$$f = \frac{C}{C_o}, \quad s = \frac{z}{L}$$

Equation 24 becomes,

$$\frac{1}{P_e} \frac{\partial^2 f}{\partial s^2} - \frac{\partial f}{\partial s} - D_a f = 0, \qquad (25)$$

where

$$P_e = \frac{vL}{D_z}, \quad D_a = \eta k \frac{L}{v}$$

Two boundaries conditions are required to solve Equation 25 analytically.

$$\text{1st B.C.} \quad \frac{\partial f}{\partial s} = Pe\ (f - 1), \quad s = 0$$

$$\text{2nd B.C.} \quad \frac{\partial f}{\partial s} = 0 \qquad , \quad s = 1$$

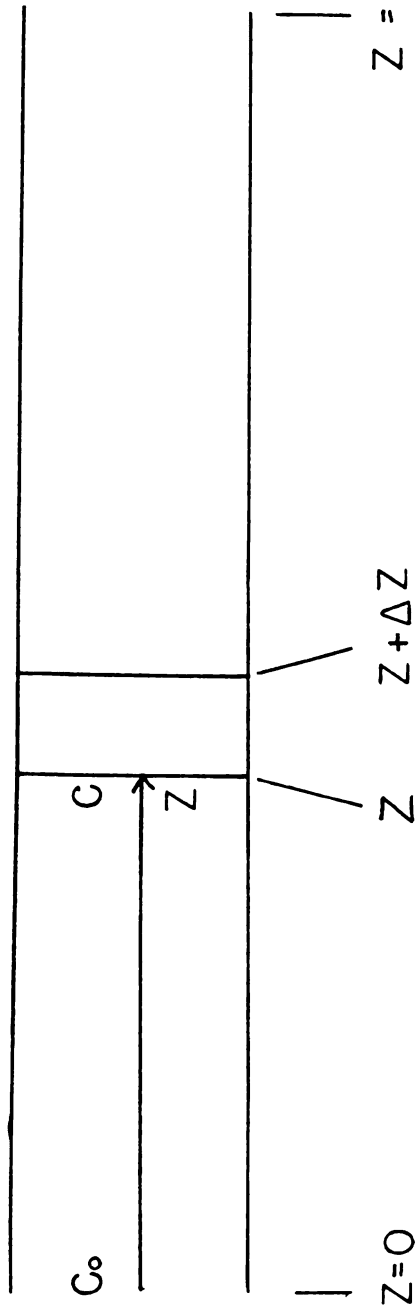

Figure 21.--Drawing of plug flow reactor showing differential element.

The solution of 25 is

$$f\ (1) = \frac{Pe}{\Delta}\ (\sqrt{Pe^2 + 4\ PeDa})\ \exp\ (Pe) \qquad (26)$$

where

$$\Delta = R_+^2\ \exp\ (R_+) - R_-^2\ \exp\ (R_-) \qquad (27)$$

$$R\pm = \frac{Pe \pm \sqrt{Pe + 4\ PeDa}}{2} \qquad (28)$$

and

$$1 - f\ (1) = X\ (\text{conversion}) \qquad (29)$$

Figures 22, 23, and 24 show the effect of a range of Peclet numbers from 0 to 14 on the conversion of steam in a tubular reactor for char particle sizes of 0.5, 1.0, and 2.0 cm. Biot mass numbers from 0.1 to 100 were used as a parameter to evaluate the effect of external mass transfer. The following values were used: $k = 1.519\ s^{-1}$, $\mathcal{D}_e = 3.19\ cm^2/s$, L = 40 cm, and v = 40 cm/s. Comparison of Figures 25, shows the effect of increasing reaction rate on steam conversion. The 625°C K_2CO_3 catalyzed rate constant of $4.464\ s^{-1}$ was used in Figure 25, with all other parameters the same. Conversion of steam is improved from 0.55 in the Na_2CO_3 catalyzed case to 0.75 in the K_2CO_3 catalyzed case for a well mixed reactor

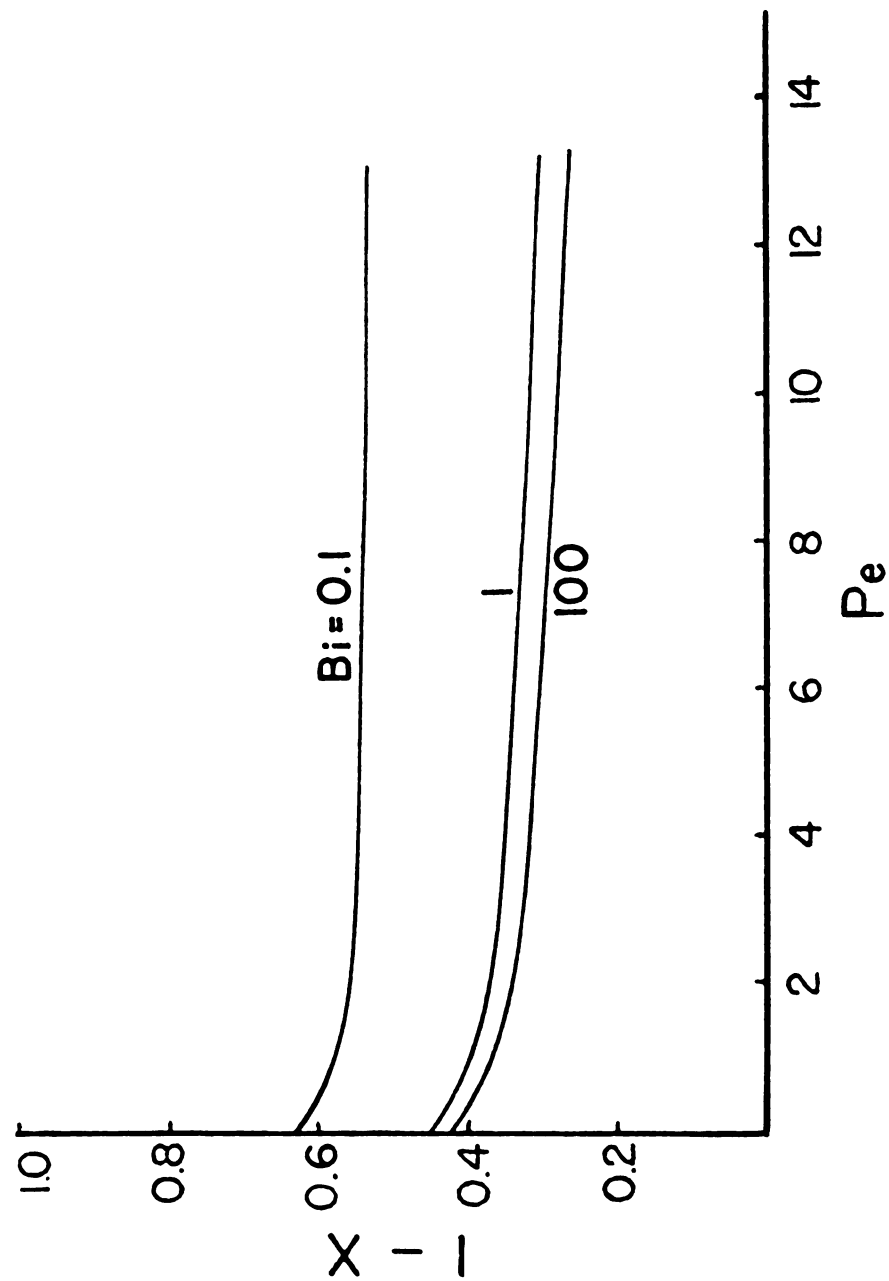

Figure 22.--Plot of 1 - X versus Pe number. $\mathcal{D}_e$ = 3.10 cm^2/sec, k = 1.519 s^{-1}, L = 40 cm, v = 40 cm, D_p = 0.5 cm.

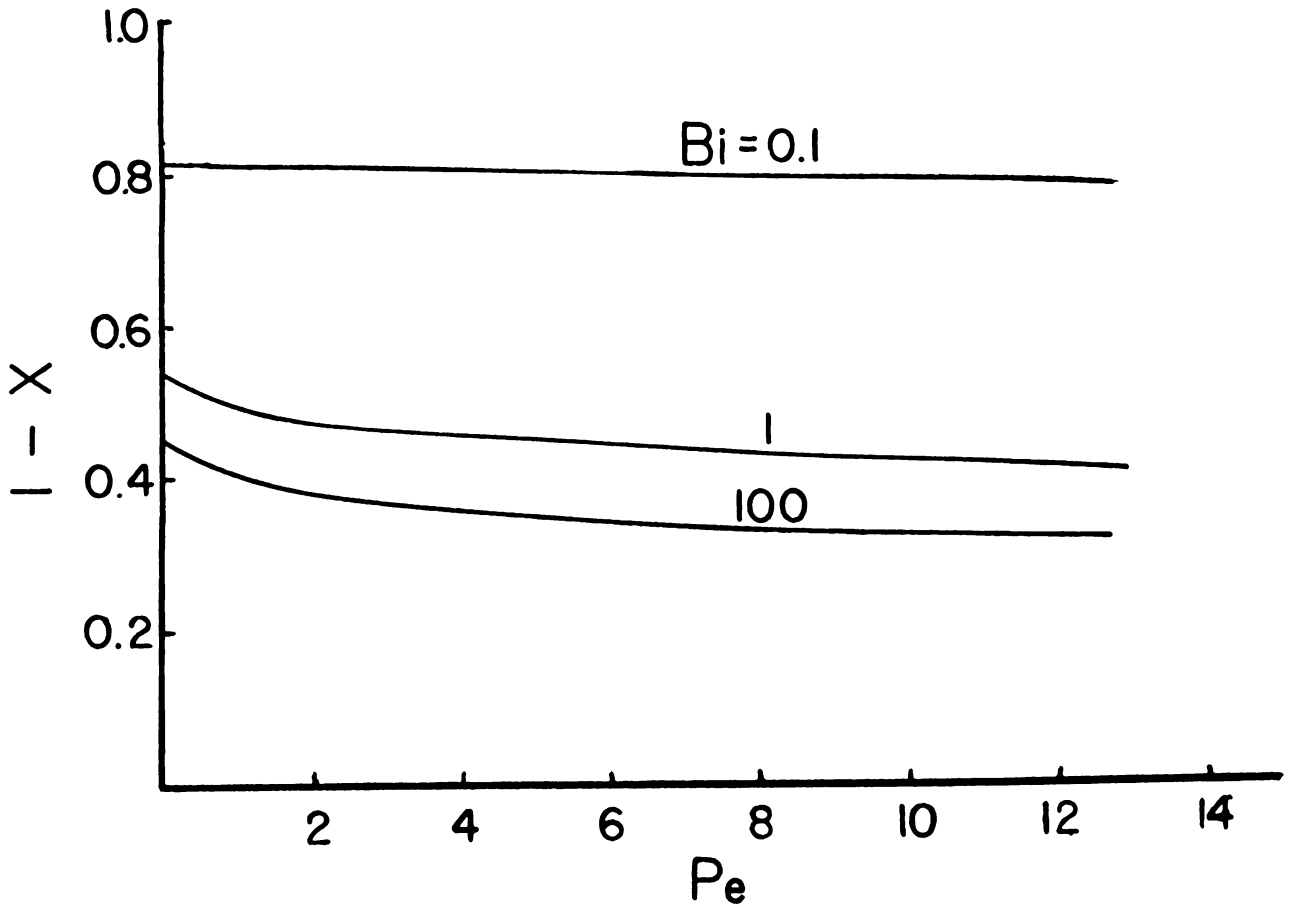

Figure 23.--Plot of 1 - X versus Peclet number. $\mathcal{D}_e$ = 3.19 cm^2/sec, k = 1.519 s^{-1}, L = 40 cm, v = 40 cm/sec, D_p = 1.0 cm.

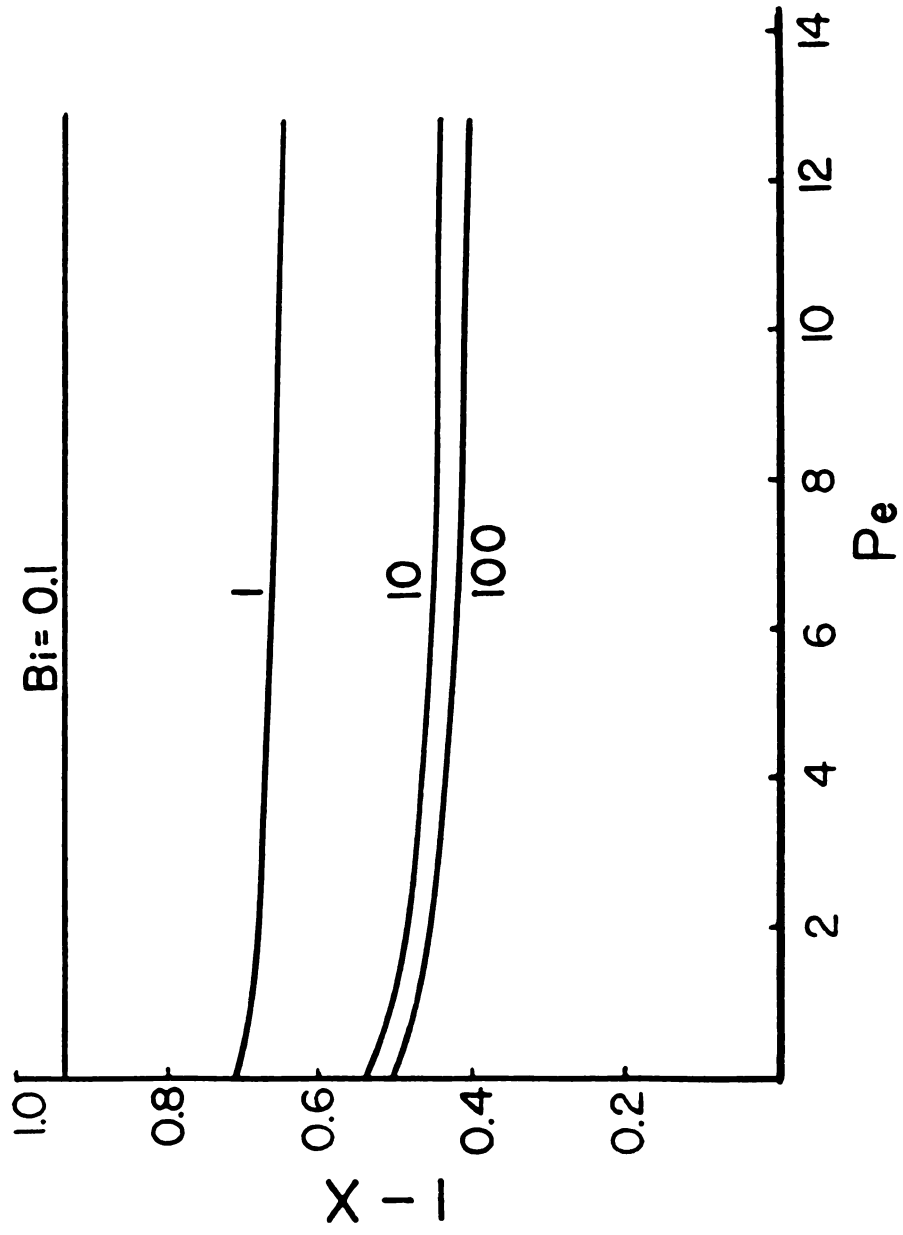

Figure 24.--Plot of 1 - X versus Peclet number. $\mathcal{D}_e$ = 3.19 cm^2/sec, k = 1.519 s^{-1}, L = 40 cm, v = 40 cm/sec, D_p = 2.0 cm.

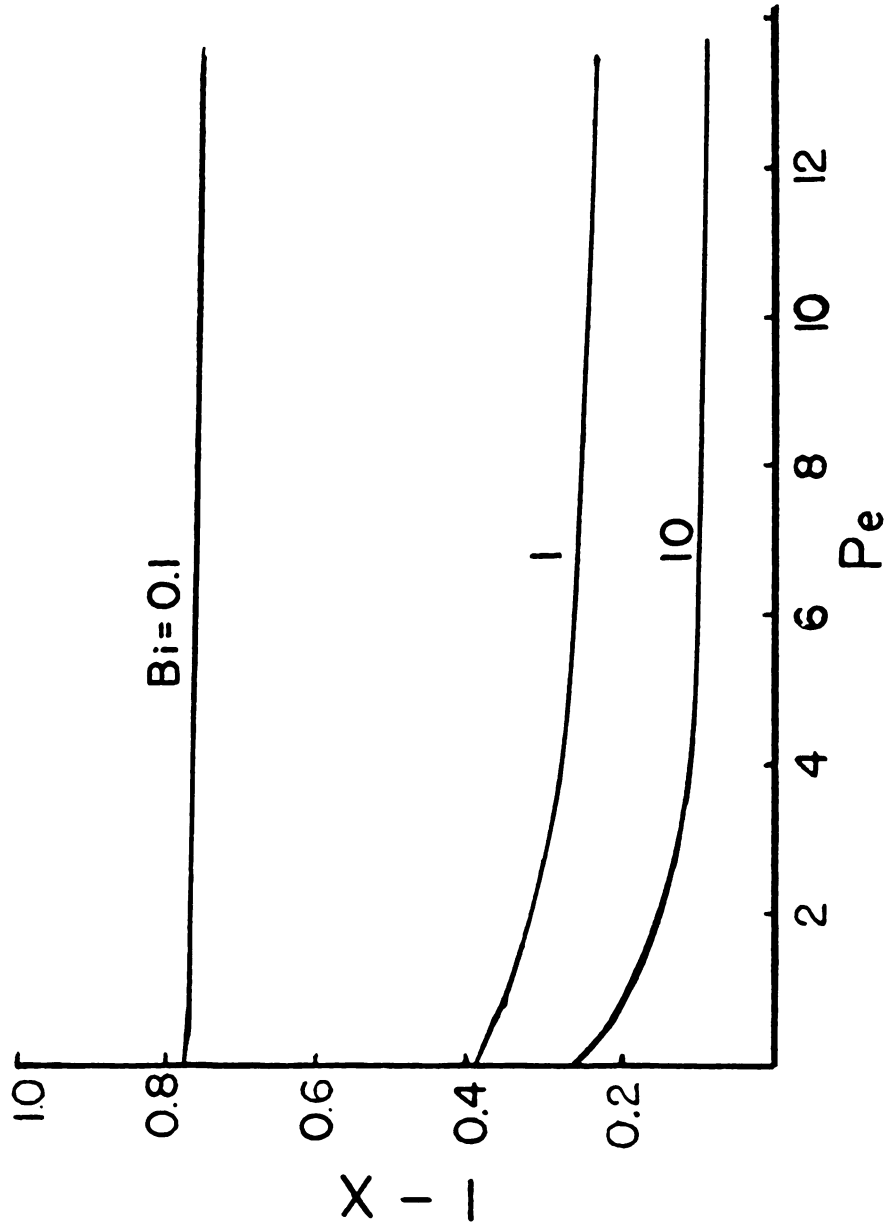

Figure 25.--Plot of 1 - X versus Peclet number. $\mathcal{D}_e$ = 3.19 cm^2/sec, k = 4.464 s^{-1}, L = 40 cm, v = 40 cm/sec, D_p = 1.0 cm.

and no external mass transfer resistance. Figure 26 shows the effect of residence time on the conversion of steam. Figure 27 demonstrates conversion as a function of effective diffusivity for a 1.0 cm particle and a rate of 1.519 s^{-1}. A limiting value of approximately 0.70 conversion is reached for values of effective diffusivity above 3.0 cm^2/s.

Results of this modeling show that there is little sensitivity on conversion by axial mixing, since conversion is independent of Peclet number above a value of 2 for nearly all the plots.

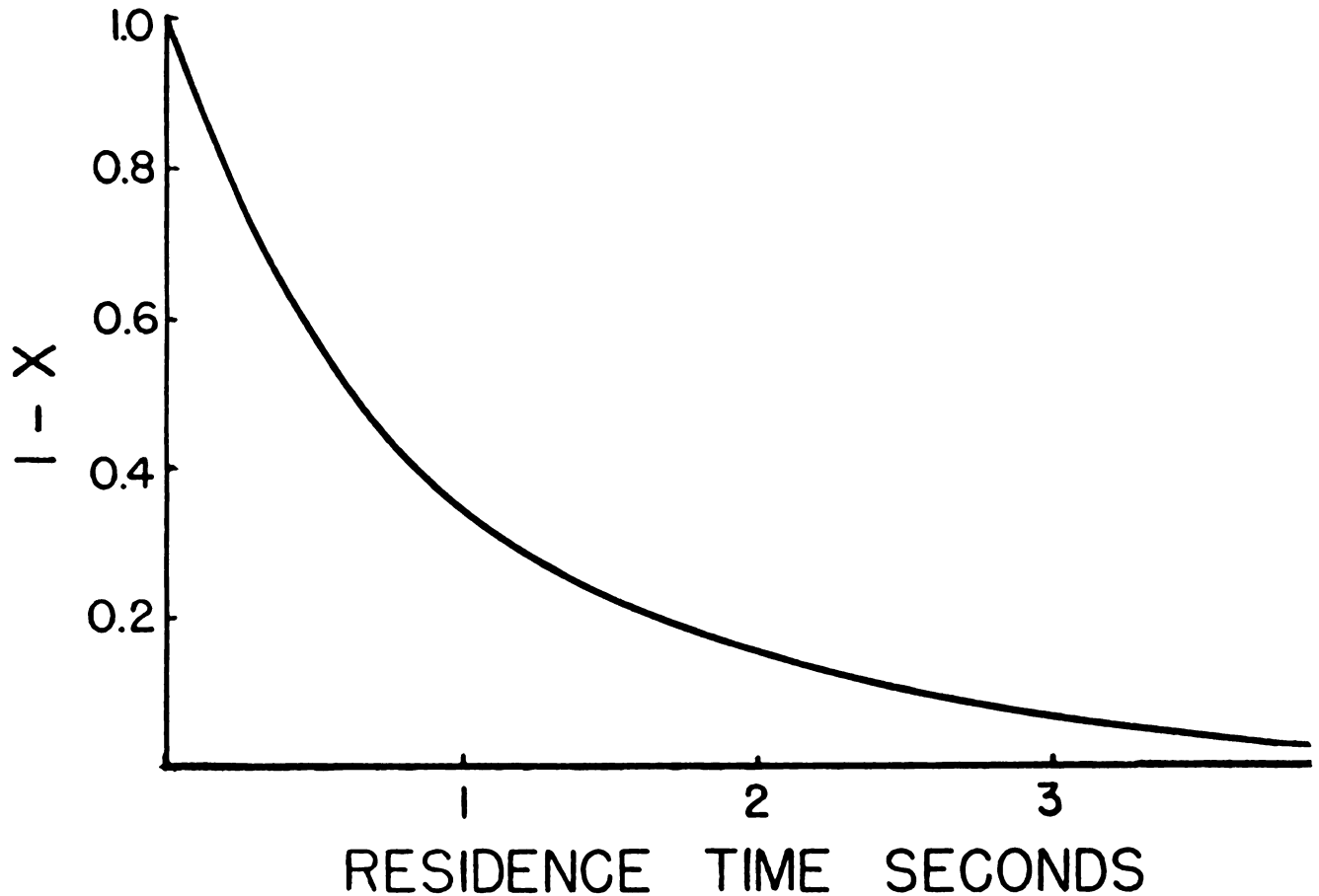

Figure 26.--Effect of residence time of steam on conversion. $\mathcal{D}_e$ = 3.19 cm^2/sec, k = 1.519 s^{-1}, L = 40 cm, D_p = 1.0 cm.

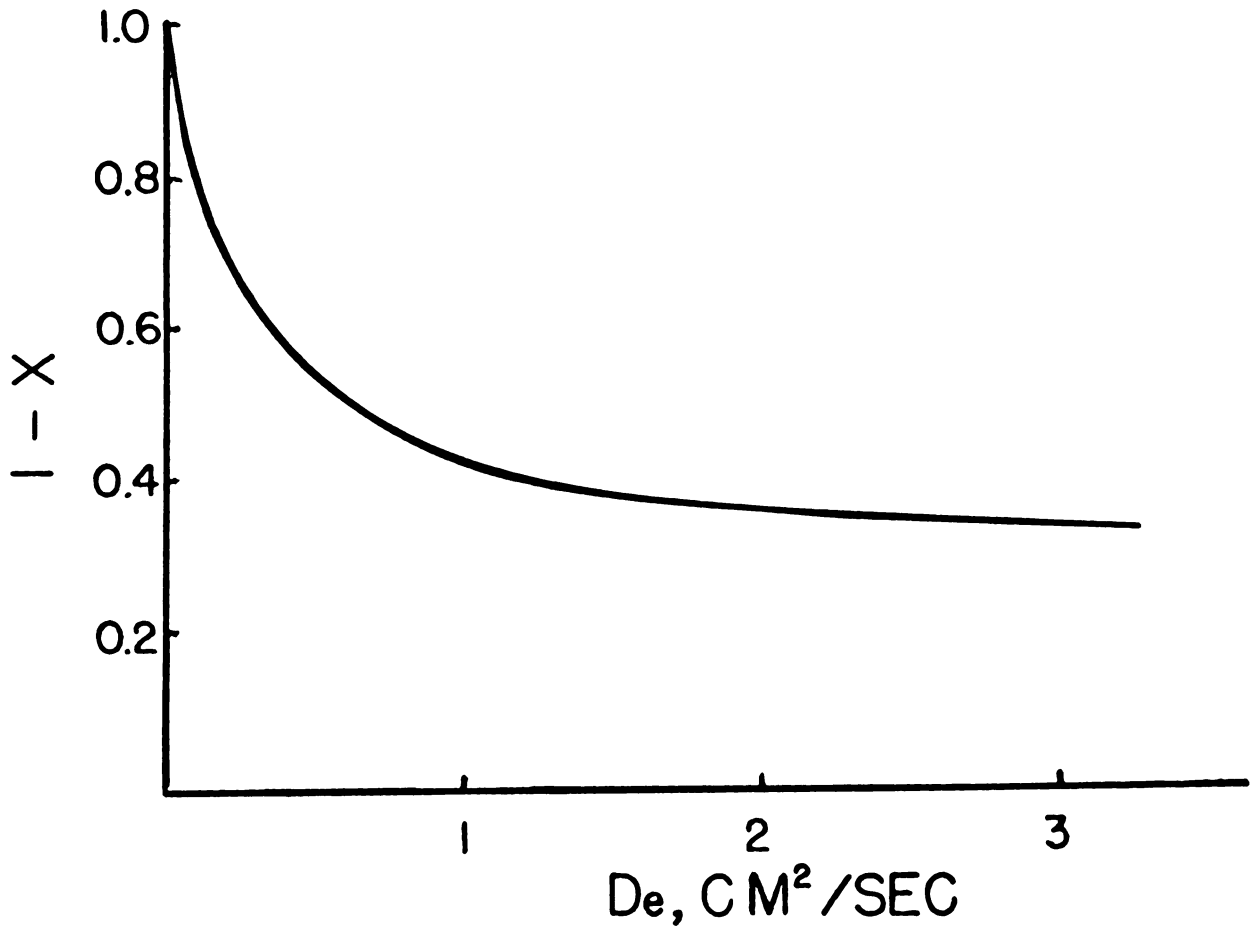

Figure 27.--Effect of effective diffusivity on conversion, k = 1.519 s^{-1}, L = 40 cm, v = 40 cm/sec, D_p = 1.0 cm.

SUMMARY AND CONCLUSIONS

Conjectures of Catalytic Activity

The influence of alkali carbonate salts on the pyrolysis of cellulosic materials and wood has been studied by several investigators (17, 19, 20). The observed effects during rapid pyrolysis of wood, of less tar production and greater char production, have also been observed in this study. It appears evident from results of this study that the salts actively degrade the chemical nature of the polymer constituents. The residual char product of the salt catalyzed wood does not have the structure of the original material. This is in definite contrast to the pyrolysis char of uncatalyzed wood which retains its shape, size, and microstructure throughout pyrolysis. The catalyzed char product looks as though a foaming action occurred throughout the entire sample. Some of the char actually becomes encrusted on the outside of the sample basket. This degradation of the wood may occur during the pretreatment step, while soaking in the salt solution, or while drying at 100°C for 24 to 48 hours. Or the degradation may occur just prior to the pyrolysis period as the material is undergoing a rapid

temperature rise. Sufficient chemical or physical degradation occurs such that the material flows. Foaming of the material may be the result of volatile alkali compounds occuring at the experimental temperatures above 600°C.

The increase in the gasification rate for char impregnated with salt as opposed to untreated char may possibly result from two different effects. The graphitic carbon structure of char provides active sites to the reacting steam molecules. The actual enhancement might possibly be the result of increasing the rate of water adsorption at the active sites, or increasing the number of active centers for the gasification reaction to occur. Increased rate of water adsorbtion may be the result of a changed charge distribution on the surface. The number of active sites would depend on how the cation chemically reacts with the surface. The alkali metal is most likely responsible for the rate increase, since the carbonate would be thermally unstable above 500°C.

Observations and Comments

The initial objective of this research was to study the catalytic gasification of Poplar SPP. Preliminary gasification experiments of dried wood over the temperature range of 400° to 700°C produced gaseous,

liquids, tars and char products. Experimental difficulties were encountered related to quantitative analysis of liquid and tar products and deposition of tars on various equipment components. Therefore the objectives of this study were revised to study the intrinsic gasification kinetics of catalyzed Poplar SPP char prepared from pyrolysis of raw wood in 700°C nitrogen for a period of 10 minutes. The catalytic activity of two different salts was investigated. Experiments were conducted for partial pressures of steam between 45 and 100 kPa for each catalyst, and temperatures of the reaction environment of 550°, 625°, and 700°C for each catalyst. Experiments were also conducted on uncatalyzed material to determine the effect of external mass transfer by observing space velocities of 2, 4, and 7.25 s^{-1}. Product gases were CO, CO_2, and CH_4, and H_2, which were analyzed by gas chromatography.

Based on results of the space velocity experiments it was concluded that external mass transfer is not controlling for the experimental conditions of 4 s^{-1} space velocity and 1 to 2 mm diameter particles. Reaction rates were calculated in two manners. For case A, it was assumed that methane was produced by direct hydrogenation of char, thus the gasification rate was calculated based on the total production of carbon oxides. In case B, it

was assumed that methane was produced by reaction of carbon monoxide and hydrogen, therefore the reaction rate is proportional to the sum of the carbon oxides and methane. Both reaction rate calculations indicate the following rate law.

$$\text{Gasification rate} = k\ (T)\ p_{H_2O}\ \frac{\text{moles}}{\text{gr C, min}} \qquad (12)$$

These results are in contrast to the results of the noncatalyzed experiments, where it appears that Langmuir-Hinshelwood kinetics may apply.

Activation energies of 84.9 kJ/mole and 94.2 kJ/mole were obtained for Na_2CO_3 and K_2CO_3 catalyzed gasification reactions, respectively. Uncatalyzed char had an activation energy of 156 kJ/mole. Averaged frequency factors found were 10.7 and 16.4 moles/gr C, min, kPa for Na_2CO_3 and K_2CO_3 catalyzed gasification reactions, respectively.

Using the observed intrinsic kinetics and an estimated effective diffusivity of steam, a particle model was developed to calculate an effectiveness factor versus particle size. The results of the calculation show the internal mass transfer becomes significant for particles larger than 0.5 cm when no external mass transfer limitations are included. The effect of external mass transfer

can be significant for any particle over 0.2 cm in width. The results of the effectiveness factor calculation were then used in an axial dispersed plug flow reactor model to estimate conversion of steam. Using estimated diffusion characteristics, a range of Peclet numbers were analyzed for particle sizes of 0.5, 1.0, and 2.0 cm in size. The results of this modeling show that there is generally little sensitivity of the system to mixing conditions within the reactor, since conversion is independent for values of the Peclet number larger than two for all particle sizes.

APPENDICES

APPENDIX A

FUTURE WORK

FUTURE WORK

1. A series of microphotographs of salt impregnated char, prior to and during pyrolysis or gasification, to examine possible structural damage to the cell walls.

2. Examination of the catalytic activity of a series of salts formed from the same alkali metal. This might give some insight on the specific chemical nature of the char catalyst interaction.

3. The affect of a range of concentrations of one salt on catalytic activity. This might provide data on the number of active sites generated on the carbon surface by the catalyst.

4. Quantitative examination of initial wood and the residual material, particularly for ash content.

5. Test a greater variety of metal compounds for possible catalytic activity on the gasification reaction.

6. Examination of the gasification reaction rate behavior for known concentrations of H_2 and CO_2, to analyze possible inhibition of the rate by these gases. To do this safely a significant change in the experimental apparatus would be required.

7. A theoretical treatment of pyrolysis reactions. This could be accomplished by lumping populations of functional groups and bonds within the material to develop a series of hypothetical reactions.

8. Extension of the experimental apparatus to enable the quantitative analysis of liquid pyrolysis products.

9. Experimental study of the gasification reaction rate kinetics of gaseous and liquid pyrolysis products derived from wood.

10. Physical characterization study of the char residue to determine accurately the pore distribution, porosity, and diffusional properties.

11. More elaborate experiments with the existing experimental apparatus, to determine the effect of space velocity on mass and heat transfer within the reaction chamber.

12. Extension of the modeling to a nonisothermal treatment, particularly for pyrolysis modeling.

13. Extension of experiments to larger particles to evaluate the previous modeling studies.

APPENDIX B

SAMPLE RATE CALCULATIONS

SAMPLE RATE CALCULATIONS

The following presents sample calculations for the experimental run with a temperature of 550°C, steam partial pressure of 100 kPa, and a space velocity of 4 s^{-1}.

Calculation of product gas composition.*

Component	Calibration factor, f_i	Peak weight, w_i
H_2	2.41	0.07475
N_2	1.00	0.18703
CO	0.96	0.00600
CH_4	0.82	0.00726
CO_2	1.53	0.02826

*The product gas compositions were averaged over all of the gas samples taken. Only the data for one gas sample is presented above.

$$\text{mol fraction}_i = \frac{f_i \, w_i}{\sum_{i=1}^{5} f_i \, w_i}$$

Component	Mol fraction	Mol fraction on nitrogen free basis
H_2	.243	.618
N_2	.607	--
CO	.019	.051
CH_4	.039	.099
CO_2	.092	.234

Calculation of material balance:

Average nitrogen flow = 0.105 ℓ/min at 25°C, 1 atm

Total measured gas flow = 2.78 ℓ at 25°C, 1 atm

- Total nitrogen flow = 1.58 ℓ at 25°C, 1 atm

Total gas flow - N_2 flow = 1.20 ℓ at 25°C, 1 atm

$$\text{Total carbon in product gas} = \frac{\text{Total gas} - N_2\ (\ell)}{\dfrac{1.0\ (\text{mol})}{24.451\ (\ell)}} \times \frac{12\ (\text{g})}{1\ (\text{mol})}$$

$$\times \text{ mol fraction of } (CO_2 + CO + CH_4)$$

$$= \frac{1.20\ (1.0)\ (12)\ (.238 + .060 + .102)}{24.451}$$

$$= 0.24 \text{ grams}$$

Total carbon consumed = 0.24 grams

$$\% \text{ error} = \frac{\text{Total carbon in product gas - Total carbon consumed}}{\text{Total carbon consumed}}$$

$$= \frac{0.24 - 0.24}{0.24}$$

$$= 0.0\%$$

Calculation of gasification rate:

$$\text{rate} = \frac{\text{Average product gas flow rate } (\ell/\text{min}) - \text{Average nitrogen flow rate } (\ell/\text{min})}{\text{Original carbon present (g)}}$$

$$\times \frac{1.0 \text{ mol}}{24.451 \ (\ell)} \Big| \frac{\text{mol fraction of } (CO + CO_2)}{}$$

$$= 3.652 \times 10^{-4} \frac{\text{mol}}{\text{g min}}$$

APPENDIX C

EFFECTIVENESS FACTOR CALCULATION

EFFECTIVENESS FACTOR CALCULATION

Given,

$$\eta = \frac{1}{L\ k_o C_o} \int_o^L k\ C\ dx \text{ and } \psi = \frac{\cosh\ \phi\xi}{\frac{\phi\ \sinh\ \phi}{Bi_m} + \cosh\ \phi}$$

$$\eta = \frac{1}{L\ k_o C_o} \int_o^L \text{rate}\ dx$$

Since $\text{rate} = \mathcal{D}_e \frac{\partial^2 C}{\partial x^2}$ then,

$$\int_o^L \text{rate}\ dx = \mathcal{D}_e \int_o^L \frac{\partial^2 C}{\partial x^2}\ dx = \mathcal{D}_e \int_o^L \frac{\partial C}{\partial x}$$

making this dimensionless,

$$\frac{\mathcal{D}_e\ C_o}{L} \int_o^1 \frac{\partial \psi}{\partial \xi} = \int_o^1 \text{rate}\ dx = \frac{C_o\ \mathcal{D}_e}{L} \left(\frac{\partial \psi}{\partial \xi}\bigg|_1 - \frac{\partial \psi}{\partial \xi}\bigg|_o\right)$$

since

$$\int^L \text{rate}\ dx = \frac{C_o\ \mathcal{D}_e}{L} \frac{\partial \psi}{\partial \xi}\bigg|_1,$$

then

$$\eta = \frac{\mathcal{D}_e}{L^2 k_o} \left.\frac{\partial \psi}{\partial \xi}\right|_1 .$$

$$\left.\frac{\partial \psi}{\partial \xi}\right|_1 = \frac{\phi \sinh \phi}{\frac{\phi \sinh \phi}{Bi_m} + \cosh \phi}$$

then substituting,

$$\eta = \frac{1}{\phi^2} \frac{\phi \sinh \phi}{\frac{\phi \sinh \phi}{Bi_m} + \cosh \phi} = \frac{\tanh \phi}{\phi\left(1 + \frac{\phi \tan \phi}{Bi_m}\right)}$$

APPENDIX D

SUMMARY OF RATE DATA

TABLE 3.--Summary of Rate Data.

	Temperature °C	Partial Pressure H_2O kPa	Observed Rate x 10^3 g mole/g min	Average Calculated Rate x 10^3 g mole/g min	Percentage Error
CASE A:					
Na_2CO_3	550	100	1.41	1.54	9
	625	98.2	5.96	4.73	20
	685	100	8.40	10.23	21
	625	98.2	5.96	6.25	4.8
	625	76.4	4.51	4.86	5.4
	625	41.0	2.86	2.60	9.6
K_2CO_3	550	100	1.74	1.74	.6
	625	98.2	5.45	5.45	.2
	700	100	14.47	14.47	0
	625	98.2	5.48	5.21	5
	625	69.5	3.98	3.68	8
	625	58.9	2.71	3.12	15

TABLE 3.--Continued.

	Temperature °C	Partial Pressure H_2O kPa	Observed Rate x 10^3 g mole/g min	Average Calculated Rate x 10^3 g mole/g min	Percentage Error
CASE B:					
Na_2CO_3	550	100	1.66	1.74	5
	625	98.2	6.12	4.92	24
	685	100	8.84	10.92	23
	625	98.2	6.12	6.84	12
	625	76.4	4.74	5.32	12
	625	41.0	3.48	2.85	23
K_2CO_3	550	100	1.91	1.82	5
	625	98.2	5.64	5.67	.5
	700	100	14.71	15.27	4
	625	98.2	5.64	6.77	20
	625	69.5	4.73	4.79	1
	625	58.9	4.79	4.06	18

TABLE 3.--Continued.

Temperature °C	Partial Pressure H_2O kPa	Observed Rate x 10^3 g mole/g min	Average Calculated Rate x 10^3 g mole/g min	Percentage Error
UNCATALYZED RUNS:				
625	99.9	3.37	3.72	10
625	88.6	3.49	3.30	6
625	63.6	2.12	2.36	11
625	46.6	1.98	1.73	14
550	100	.365	.413	9.3
685	100	8.90	10.21	12.8

	Space Velocity $Second^{-1}$	Observed Rate x 10^3 g mole/g min	Average Calculated Rate x 10^3 g mole/g min	Percentage Error
SPACE VELOCITY EXPERIMENTS:				
(Temperature = 625°C) (Steam Partial Pressure = 100 kPa	2	3.43	3.37	2
	4	3.37	3.37	0
	7.25	2.27	3.37	48

BIBLIOGRAPHY

BIBLIOGRAPHY

1. Anonymous, "Biomass Potential in 2000 put at 7 quads," Chem. Eng. News, February 12, 1979, pp. 20-22.

2. Brenden, J.J., "Caloric Values of the Volatile Pyrolysis Products of Wood," Combustion and Flame, 11, 4, pp. 437-439, 1967.

3. Roberts, A.F. and Glough G., "Thermal Decomposition of Wood in an Inert Atmostphere," Ninth Symposium (International) on Combustion, pp. 158-166, 1963.

4. Kanury, A.M., "Thermal Decomposition Kinetics of Wood Pyrolysis," Combustion and Flame, 18, pp. 75-83, 1972.

5. Blackshear, Jr., P.L. and Murty, K.A. "Heat and Mass Transfer to, from, and within Cellulosic Solids Burning in Air," Ninth Symposium (International) on Combustion, pp. 910-923, 1965.

6. Beall, F.C., "Differential Calorometric Analysis of Wood and Wood Components," Wood Science and Technology, 5, pp. 159-175, 1971.

7. Arseneau, D.F., "The Differential Thermal Analysis of Wood," Can. J. Chem., 39, pp. 1915-1919, 1961.

8. Lipska, A.E. and Parker, W.J., "Kinetics of the Pyrolysis of Cellulose in the Temperature Range 250°-350°C," J. of Applied Polymer Science, 10, pp. 1439-1453, 1966.

9. Madrosky, S.L., Hart, F.G., and Straus, S., "Pyrolysis of Cellulose in a Vacuum," J. Res. Natl. Bur. Std., 56, 343, 1956.

10. Chatterjee, P.K. and Conrad, C.M., "Kinetics of the Pyrolysis of Cotton Cellulose," Textile Research Journal, 36, pp. 487-494, 1966.

11. Golova, O.P. and Krylona, R.G., "Thermal Decomposition of Cellulose and its components," Dokl. Akad. Nauk SSR, 116, pp. 419, 1957. Chem. Abstracts, 52, pp. 4979, 1958.

12. Beall, F.C., "Thermogravimetric Analysis of Wood Lignin and Hemicelluloses," Wood and Fiber, 1, pp. 215-226, 1969.

13. Stamm, A.J., "Thermal Degradation of Wood and Cellulose," Ind. and Eng. Chem., 48, pp. 413-417, 1956.

14. Shafizadeh, F., "Pyrolysis and Combustion of Cellulose Materials," Advan. Carbohydrate. Chem., 23, pp. 419-74, 1968.

15. Browne, F.L., "Theories of the Combustion of Wood and its Control," Forests Products Laboratory Report 2136, 1958.

16. Blackwood, J.D. and McGrory, F., "The Carbon-Steam Reaction at High Pressure," Aust. J. Chem., 11, pp. 16-33, 1958.

17. Lewis, W.K., Gilliland, E.R., and Hipkin, H., "Carbon-Steam Reaction at Low Temperatures," Ind. Eng. Chem., 45, pp. 1697-1703, 1953.

18. Stern, E.W., Logiudice, A.S., and Heinemann, H., "Approach to Direct Gasification of Cellulosics," Ind. Eng. Chem., Process Design and Development, 4, pp. 171-173, 1965.

19. Garten, R.L., "Catalytic Conversion of Biomass to Fuels," Paper presented at the Second Annual Fuels from Biomass Symposium, Troy, New York, June 20, 1978.

20. Walkup, P.C., Mudge, L.K., Cox, J.L., Sealock, L.J., and Roberts, R.J., "Investigation of Biomass in the Presence of Multiple Catalysts," Paper presented at Second Annual Fuels from Biomass Symposium, Troy, New York, June 20, 1978.

21. Shafizadeh, F. and McGinnis, "Morphology and Biogenisis of Cellulose and Plant Cell Walls," Advan. Carbohydrate Chem. Biochem, 307-312, 1971.

22. Bird, R.B., Stewart, W.E., and Lightfoot, E.W., Transport Phenomena, Wiley, New York, 1960, Eg. 184-25, p. 571.

23. Panshin, A.J. and DeZeeuw, C., Textbook of Wood Technology, McGraw-Hill, New York, 1970, p. 217.

24. Wakoo, N. and Smith, I.M., "Diffusion in Catalyst Pellets," Chem. Eng. Sci., 17, p. 825, 1962.